

Identifying Electronic Properties Relevant to Improving the Performance and Stability of Amorphous Silicon-Based Mid-Gap and Low-Gap Cells

**Annual Subcontract Report
16 January 1998 —15 January 1999**

J.D. Cohen

*Department of Physics and Materials Science Institute
University of Oregon
Eugene, Oregon*



NREL

National Renewable Energy Laboratory

1617 Cole Boulevard
Golden, Colorado 80401-3393

NREL is a U.S. Department of Energy Laboratory
Operated by Midwest Research Institute • Battelle • Bechtel

Contract No. DE-AC36-99-GO10337

Identifying Electronic Properties Relevant to Improving the Performance and Stability of Amorphous Silicon-Based Mid-Gap and Low-Gap Cells

**Annual Subcontract Report
16 January 1998 —15 January 1999**

J.D. Cohen

*Department of Physics and Materials Science Institute
University of Oregon
Eugene, Oregon*

NREL Technical Monitor: B. Von Roedern

Prepared under Subcontract No. PV005001



NREL

National Renewable Energy Laboratory

1617 Cole Boulevard
Golden, Colorado 80401-3393

NREL is a U.S. Department of Energy Laboratory
Operated by Midwest Research Institute • Battelle • Bechtel

Contract No. DE-AC36-99-GO10337

NOTICE

This report was prepared as an account of work sponsored by an agency of the United States government. Neither the United States government nor any agency thereof, nor any of their employees, makes any warranty, express or implied, or assumes any legal liability or responsibility for the accuracy, completeness, or usefulness of any information, apparatus, product, or process disclosed, or represents that its use would not infringe privately owned rights. Reference herein to any specific commercial product, process, or service by trade name, trademark, manufacturer, or otherwise does not necessarily constitute or imply its endorsement, recommendation, or favoring by the United States government or any agency thereof. The views and opinions of authors expressed herein do not necessarily state or reflect those of the United States government or any agency thereof.

Available electronically at <http://www.doe.gov/bridge>

Available for a processing fee to U.S. Department of Energy
and its contractors, in paper, from:

U.S. Department of Energy
Office of Scientific and Technical Information
P.O. Box 62
Oak Ridge, TN 37831-0062
phone: 865.576.8401
fax: 865.576.5728
email: reports@adonis.osti.gov

Available for sale to the public, in paper, from:

U.S. Department of Commerce
National Technical Information Service
5285 Port Royal Road
Springfield, VA 22161
phone: 800.553.6847
fax: 703.605.6900
email: orders@ntis.fedworld.gov
online ordering: <http://www.ntis.gov/ordering.htm>



PREFACE

This Annual Technical Progress Report covers the work performed at the University of Oregon for the period 16 January 1998 to 15 January 1999 under NREL Subcontract Number XAF-8-17619-05. The following personnel participated in this research program:

NAME	TITLE	WORK PERFORMED
J. David Cohen	Principal Investigator	Program Manager
Yoram Lubianiker	Research Associate	Studies of degradation in mixed-phase dc sputtered material; studies of H-diluted a-Si:H films; Properties of high deposition rate a-Si:H.
Chih-Chiang Chen	Research Assistant	Defect properties of a-Si _x Ge _{1-x} :H Alloys;
Kimon Palinginis	Research Assistant	Defect properties of low Ge fraction a-Si _x Ge _{1-x} :H alloys
Yanyang Tan	Research Assistant	Properties of a-Si:H samples deposited at high rates.

TABLE OF CONTENTS

	Page
LIST OF ILLUSTRATIONS	iii
LIST OF TABLES	iv
EXECUTIVE SUMMARY	v
 1.0 INTRODUCTION	 1
2.0 SAMPLES	
2.1 MIXED PHASE SAMPLES PRODUCED BY DC MAGNETRON SPUTTERING	2
2.2 HIGH GROWTH RATE SAMPLES PRODUCED AT ETL	3
2.3 HIGH GROWTH RATE SAMPLES PRODUCED AT UNI-SOLAR	3
2.4 AMORPHOUS SILICON AT THE EDGE OF MICROCRYSTALLINITY	4
2.5 GLOW DISCHARGE AMORPHOUS SILICON-GERMANIUM ALLOYS	4
 3.0 EXPERIMENTAL CHARACTERIZATION METHODS	
3.1 ADMITTANCE SPECTROSCOPY	5
3.2 DRIVE-LEVEL CAPACITANCE PROFILING	5
3.3 TRANSIENT CAPACITANCE SPECTROSCOPY	6
3.4 TRANSIENT PHOTOCAPACITANCE AND PHOTOCURRENT	7
 4.0 LIGHT INDUCED DEGRADATION KINETICS IN MIXED PHASE SAMPLES	 8
4.1 EVIDENCE FOR PRESENCE OF MICROCRYSTALLINE COMPONENT	8
4.2 BEHAVIOR OF LIGHT INDUCED DEFECT CREATION	10
4.3 MODELING	12
 5.0 DEFECT BEHAVIOR OF a-Si:H NEAR THE MICROCRYSTALLINE ONSET	 16
 6.0 CHARACTERIZATION OF HIGH GROWTH RATE a-Si:H MATERIAL	 20
6.1 ETL HIGH GROWTH RATE SAMPLES	20
6.2 UNI-SOLAR HIGH DEPOSITION RATE a-Si:H FILMS	23
 7.0 DEFECT DENSITIES IN THE AMORPHOUS SILICON-GERMANIUM ALLOYS	 26
 8.0 SUMMARY AND CONCLUSIONS	 30
 9.0 SUBCONTRACT SUPPORTED PUBLICATIONS	 31
 10.0 REFERENCES	 32

LIST OF ILLUSTRATIONS

	Page
FIG. 1. Schematic diagram indicating the basic sequence of events in semiconducting junction transient measurements	7
FIG. 2 Raman spectrum for Illinois, dc sputtered sample 1937	8
FIG. 3. Bright-field TEM image of Illinois sample 1921	9
FIG. 4. Photocapacitance spectrum of Illinois sample 1937 showing a “crystalline silicon” feature	9
FIG. 5. Drive-level capacitance profiling defect densities obtained as a function of light soaking time	11
FIG. 6. Defect density as a function of light soaking time for various light intensities	12
FIG. 7. The defect density as a function of the annealing temperature.....	12
FIG. 8. The third power of the defect density as a function of light soaking time	13
FIG. 9. Defect density vs. light soaking time: experiment and model.....	15
FIG. 10. Drive-level capacitance profiles for the Uni-Solar standard glow discharge sample in its light degraded state.....	17
FIG. 11. Drive-level capacitance profiles for the two hydrogen diluted Uni-Solar standard glow discharge samples in their light degraded state	18
FIG. 12. Comparison of drive-level profiles for all three samples at the highest profiling temperatures.	18
FIG. 13. Photocapacitance spectra for the two Uni-Solar hydrogen diluted a-Si:H samples of different thickness.....	19
FIG. 14. Deep defect density for the ETL a-Si:H films in both their dark annealed state A, and a light degraded state B.....	21
FIG. 15. Deep defect density vs. light exposure for ETL a-Si:H sample grown under hydrogen dilution	21
FIG. 16. Sub-band-gap, photocapacitance spectrum of the hydrogen diluted sample showing a feature due to a small component of silicon microcrystallites	22

FIG. 17.	Photocapacitance spectra for the non diluted samples	22
FIG. 18.	Drive-level capacitance profiles for three Uni-Solar a-Si:H samples in their light degraded states.....	24
FIG. 19.	Sub-band-gap spectra obtained from transient photocapacitance measurements of the three Uni-Solar samples in their light degraded state.....	25
FIG. 20.	Urbach energies vs. Ge content determined from sub-band-gap spectra for a-Si,Ge:H samples taken from different studies.....	26
FIG. 21.	Defect densities vs. Ge content determined from ESR measurements and capacitance profiling studies.....	27
FIG. 22.	Measured defect densities vs. the value predicted from the spontaneous bond-breaking model of M. Stutzmann.....	28
FIG. 23.	Measured charged defect densities vs. the value predicted from the modified spontaneous bond-breaking model for Uni-Solar 35at.% Ge samples.....	29

LIST OF TABLES

TABLE I.	The growth parameters and characteristics of the ETL samples.....	3
TABLE II.	Properties deduced for Uni-Solar a-Si:H samples of varying deposition rate....	24

EXECUTIVE SUMMARY

The work carried out under NREL Subcontract Number XAF-8-17619-05 has concentrated on four areas of study. We first report results on a set of samples produced by dc reactive magnetron sputtering by John Abelson's group at the University of Illinois, for which we demonstrated the existence of a small but significant microcrystalline component. For these films the degradation kinetics were found to be quite unusual; however, they could be accounted for by a model that postulated two phases of degrading material: (1) a-Si:H host material of good quality and (2) a more defective component associated with boundary regions near the microcrystallites. Our sub-band-gap photocapacitance measurements on these films also indicated the existence of a distinct feature (a "shoulder" with a threshold near 1.1eV) that signaled the presence of the microcrystalline phase. The second study examined a set of samples produced by Uni-Solar which were deposited under conditions of high hydrogen dilution just below the microcrystalline phase boundary. Here we found that the defect density following light-induced degradation decreased as the film thickness increased. Corroborating our findings with X-ray diffraction (XRD) results obtained by Don Williamson on sets of similar films, we concluded that the films were becoming more ordered and less defective just prior to the onset of a detectable microcrystalline component. Furthermore we found that under conditions where XRD provided evidence for the onset of microcrystallinity, we likewise found the appearance of the distinctive microcrystalline "shoulder" in our sub-band-gap photocapacitance spectra. Third, we investigated two sets of samples where the deposition rate had been varied to include samples grown at moderate to high rates. In one set of samples, produced at Electrotechnical Laboratory in Japan, samples deposited under H₂ dilution at 10Å/sec were found to exhibit extremely low deep defect densities and narrow Urbach tails, indicating films of exceptional quality. The photocapacitance spectra for these films were found to contain evidence for a small degree of microcrystallinity. In another set of samples, produced at Uni-Solar, we found evidence for increasing defect densities plus somewhat larger Urbach energies for the films deposited at higher rates. This is consistent with the fact that the photovoltaic device performance is significantly poorer for the higher deposition rate material. Finally, we discussed the general issue of deep defect densities in the a-Si,Ge:H alloys. We again demonstrated how well the deep defect densities in such samples from several sources could be fit using the spontaneous bond-breaking model of Martin Stutzmann. This implies that such state-of-the-art alloy films have been optimized in a quantifiable sense. We also found that the increase in deep defect density with small amounts of P and B dopants could also be reproduced reasonably well by modifying the spontaneous bond-breaking model to include the extra energy terms associated with charged defects.

1.0 INTRODUCTION

The work carried out in Phase I under NREL Subcontract XAF-8-17619-05 has concentrated on four general types of studies. First, we have examined how light induced defect creation proceeds in dc reactively sputtered samples produced in John Abelson's laboratory at the University of Illinois. Previous studies have shown that these films correspond to a mixed phase between amorphous silicon and crystalline silicon with a low volume fraction of the latter. The degradation of these samples was found to be quite anomalous, and we have been able to successfully explain this in terms of a two phase degradation model.

Second, we have studied a-Si:H samples deposited under high hydrogen dilution and different growth rates. Series of such samples were obtained from Gautam Ganguly while he was still working at the Electrotechnical Laboratory (ETL) in Japan, and from United Solar Systems Corporation ("Uni-Solar"). Both sets of samples exhibited relatively low levels of degradation compared to standard glow discharge a-Si:H. In the case of the ETL samples, series of samples with and without hydrogen dilution were deposited at several different levels of rf power. The undiluted samples reveal an increasing trend toward microcrystallinity as the growth rate was decreased, while the diluted samples all reveal comparable microcrystalline levels. Some preliminary results from a series of three Uni-Solar a-Si:H samples deposited with large varying growth rates were also obtained.

Third, we participated in a three-way collaboration with Uni-Solar and Colorado School of Mines (Don Williamson's group) to examine a-Si:H samples deposited with hydrogen dilution at a level that put this material just at the edge of microcrystallite formation. It has been proposed that such samples may exhibit the absolute best stability with respect to light-induced degradation. By correlating our measurements of defect densities profiles with X-ray diffraction (XRD) measurements carried out for films of differing thickness by the CSM group, this study clearly indicates that degradation is decreased as the onset to microcrystalline phase transition is approached. Moreover, these conclusions on the film based measurements were corroborated by Uni-Solar with respect to the performance on a set of matching p-i-n devices.

Finally, we attempted to fit our experimental results for defect densities in the Uni-Solar a-Si,Ge:H alloys with a modified spontaneous defect formation model. Our previously reported results on this series of samples had indicated significant densities of charged deep defects and also had included some results for samples that were doped both n and p-type at minute levels. We had previously established that the defect levels in all the a-Si,Ge:H samples we had characterized from several independent sources quite closely obeyed the spontaneous bond breaking model proposed in 1989 by M. Stutzmann. While this model was formulated for

intrinsic material, it is quite straightforward to modify it for the case of modestly doped material. Thus we could predict the positively and negatively charged defect densities as a function of Fermi level position. This was found to provide a quite satisfactory fit to the experimental data.

In the Sections that follow, we first describe the samples studied and then briefly review the experimental techniques employed. In Section 4 we discuss our results concerning degradation in the dc magnetron sputtered mixed phase a-Si:H material obtained from the University of Illinois. In Section 5 we present our results on the high growth rate material obtained from ETL and Uni-Solar. In Section 6 we review our part in the collaborative studies to correlate sample properties just below the onset of crystalline formation. In Section 7 we will present our results fitting defect densities in the Uni-Solar a-Si_{0.8}Ge_{0.2}H to the modified spontaneous bond breaking model and, finally, in Section 8 we will summarize our findings and try to draw some general detailed conclusions.

2.0 SAMPLES

2.1 MIXED PHASE SAMPLES PRODUCED BY DC MAGNETRON SPUTTERING

Both hydrogenated and deuterated films were deposited at a rate of 100Å/min by dc reactive magnetron sputtering of a 5"×12" planar Si target in an Ar + H₂ or Ar + D₂ plasma. The substrate temperature was 250°C, the Ar partial pressure was 0.14 Pa, and the H₂ or D₂ pressure was varied from 0.04 to 0.10 Pa. Films grown under such conditions using hydrogen have been found to have properties fully equivalent to a-Si:H deposited by plasma CVD.[1] Previous studies have determined that the transition from a-Si:H to fully μ c-Si growth occurs at a hydrogen partial pressure of 0.5 Pa [2], and roughly a factor of two lower for deuterium.[3]

For the photocapacitance and photocurrent studies described below we evaporated semitransparent Pd contacts onto each film and reverse biased the junction at the p⁺ c-Si substrate. Samples were studied in "state A" (annealed in the dark at 470K for 30 minutes) and in a light soaked "state B", produced by exposure to a tungsten-halogen light source at an intensity of 300mW/cm² for 150 hours.

We previously utilized Raman spectroscopy to establish the existence of a μ c-Si component for each of these samples.[4] This method also allowed us estimate the relative volume fractions of crystallites in these samples. More information about the detailed structure of these films was obtained using high resolution plan-view TEM micrographs on a couple of the films. From such micrographs we identify a moderate density of crystallites with sizes in the 5 to 50nm range.

2.2 HIGH GROWTH RATE SAMPLES PRODUCED AT ETL

Intrinsic a-Si:H films were grown using rf plasma decomposition of silane at a substrate temperature of 250°C. One set of samples was deposited from pure silane at a pressure of 20 mTorr with a gas flow of 30 sccm. The rf power was varied (in the range of 10 to 100 Watts), thus affecting the growth rate. Another set of samples was deposited from hydrogen diluted silane in a 4:1 ratio. The silane flow was kept the same as in the first set, so that the total pressure in the chamber was 100 mTorr. In this case the H₂ dilution results in only small decrease of growth rate. For comparison we also grew a non-diluted sample at the higher pressure. The growth conditions are summarized in Table I. More details on the growth system and conditions and more information about these samples are given in ref. 5.

TABLE I. The growth parameters and characteristics of the ETL samples. In all cases the silane flow was 30 sccm.

Sample	H ₂ flow (sccm)	pressure (mTorr)	rf power (Watts)	thickness (μm)	growth rate (Å/sec)
12451	none	100	20	2.13	14.9
12464	120	100	100	2.1	15.22
12465	none	20	100	2.33	16.2
12466	120	100	60	1.9	10.55
12467	none	20	60	1.6	10.3
12468	120	100	20	1.64	2.5
12469	none	20	10	1.69	2.8

2.3 HIGH GROWTH RATE SAMPLES PRODUCED AT UNI-SOLAR

An initial series of three a-Si:H samples was obtained from Uni-Solar: one low growth rate reference film was deposited using hydrogen dilution at 1Å/sec under conditions that have produced the most stable, highest efficiency devices produced at Uni-Solar. The other two samples were deposited at 3Å/sec and 6Å/sec. The first of these was deposited in a conventional PECVD reactor utilizing modified deposition conditions (higher rf power, etc.), while the second was deposited under VHF conditions using a 70MHz excitation frequency. Both films were deposited under conditions that have led to the best performing cells reported to date for these higher deposition rates. In each case the film was deposited on a stainless steel substrate over a thin contacting layer of n⁺ a-Si:H. A Pd Schottky contact was deposited onto the top surface of each sample to enable characterization by our junction capacitance methods.

2.4 AMORPHOUS SILICON AT THE EDGE OF MICROCRYSTALLINITY

Several series of undoped (i) films were produced at Uni-Solar by PECVD at varying levels of H-dilution and film thickness (0.5 to 2.5 μm), all at a deposition temperature of 300°C. These samples were employed in a 3-way collaboration to correlate X-ray diffraction structural measurements (carried out at Colorado School of Mines), junction capacitance spectroscopic measurements of defect densities and distribution (University of Oregon), and p-i-n device performance (Uni-Solar). The substrates included bare stainless steel (i/SS), amorphous n-layer-coated stainless steel (i/a-n/SS), and microcrystalline n-layer-coated stainless steel (i/ μc -n/SS). The n-layers were typically about 20 nm thick. Solar cells of 0.05 cm^2 area for determining V_{oc} were obtained by depositing a top p-layer onto the films with an n-layer at the substrate. Three films were prepared for our drive-level capacitance profiling (DLCP): one with no H-dilution (i/a-n/SS, 1.3 μm thick) and two with high-H-dilution but different i-layer thickness' (i/a-n/SS, 1.05 μm and 1.3 μm). The level of H-dilution used in the "high-H-dilution" i-layers of the present studies were similar to the levels used in recent high-efficiency solar cells [6].

2.5 GLOW DISCHARGE AMORPHOUS SILICON-GERMANIUM ALLOYS

During our previous subcontract period we obtained nine a-Si_xGe_{1-x}:H films deposited by the rf glow discharge method at United Solar Systems Corporation. We utilized these samples for studying the deep defect structure in these alloys. All of these films were deposited on heavily p-type doped crystalline Si substrates at 300°C using mixtures of Si₂H₆ and GeH₄ gases diluted in H₂. The GeH₄ flow rate was varied to obtain different Ge fractions. Additional details of the deposition conditions have been described elsewhere [7]. The Ge fractions were determined by electron microprobe measurements, courtesy of Harv Mahan and Alice Mason at NREL. Seven of the samples studied had Ge fractions in the range 30 to 35at.%, considered the most suitable for the low gap alloy of tandem solar cells. (The remaining two samples had Ge fractions near 20at.% and 50at.%, respectively.) Five of these samples were undoped, one was n-type doped at with PH₃ at 2 ppm by gas volume (Vppm), and one was p-type doped at a level of 6Vppm BF₃.

In the current Subcontract period, although no new measurements on these films are to be reported, we tested the defect densities we had previously determined for these samples against a modified version of the spontaneous bond-breaking model. In this modified version, additional energy terms are incorporated to take into account the formation of charged defects for material that is not strictly intrinsic.

3.0 EXPERIMENTAL CHARACTERIZATION METHODS

The measurements employed in our studies rely on a set of experimental techniques which have all been described previously in some detail. They consist of (1) admittance spectroscopy as a function of temperature and frequency, (2) drive-level capacitance profiling, (3) transient capacitance spectroscopy, and (3) transient photocapacitance taken together with transient junction photocurrent spectroscopy. For the purpose of this report we will describe each method only very briefly and review what kind of information is obtained from each type of measurement.

3.1 ADMITTANCE SPECTROSCOPY

Our Schottky diode samples contain a depletion region which is characterized as a function of temperature and frequency before we undertake the more sophisticated capacitance based measurements described in Sections 3.2 to 3.4 below. Such measurements provide us with an estimate of our film thickness (the temperature independent capacitance region at low T is simply related to the geometric thickness, d , by the formula $C = \epsilon A/d$), and an Arrhenius plot of the frequency of the lowest temperature capacitance step (or conductance peak) vs. $1/T$ provides us with the activation energy of the ac conductivity, E_{σ} , which we identify with the Fermi energy position: $E_{\sigma} = E_C - E_F$. [8] These admittance measurements also give us an indication of the quality of our Schottky barriers which allow us to pre-screen our samples for further study.

3.2 DRIVE-LEVEL CAPACITANCE PROFILING

The drive-level capacitance profiling method has been described in detail in many publications [9,10]. It is similar to other kinds of capacitance profiling in that it provides us with a density vs. distance profile; however, this particular method was developed specifically to address the difficulties encountered in interpreting capacitance measurements in amorphous semiconductors. In this method we monitor the junction capacitance both as a function of DC bias, V_B , and as a function of the amplitude of the alternating exciting voltage, δV . One finds that to lowest order this dependence obeys an equation of the form:

$$C(V_B, \delta V) = C_0(V_B) + C_1(V_B) \delta V + \dots$$

and that the ratio

$$N_{DL} \equiv \frac{C_0^3}{2q_e \epsilon A^2 C_1} \quad (1)$$

is directly related to an integral over the density of mobility gap defect states:

$$N_{DL} = \int_{E_c - E_e}^{E_F^0} g(E) dE \quad (2)$$

Here E_F^0 is the bulk Fermi level position in the sample and E_e depends on the angular frequency ω and temperature of measurement:

$$E_e(\omega, T) = k_B T \log(v/\omega) \quad (3)$$

The thermal emission prefactor v has a value of roughly $2 \times 10^{13} \text{ s}^{-1}$. Thus, by altering the measurement temperature (or frequency) we obtain information about the energy distribution of the defects and, by altering the applied DC bias, we can vary the spatial region at which we detect the defects in the sample. That is, we can spatially profile the defects as a function of the position from the barrier interface.

In our current studies we typically measured 10 or 100Hz profiles for a series of temperatures between 320K to 360K. These data usually indicated a clear upper limit for N_{DL} which, we have shown [11], is equal to roughly one half the total defect density in these samples. This thus provides us with a quantitative measurement of the deep defect levels. In addition, because of the profiling information also obtained, we are able to assess the spatial uniformity of the electronic properties in these samples.

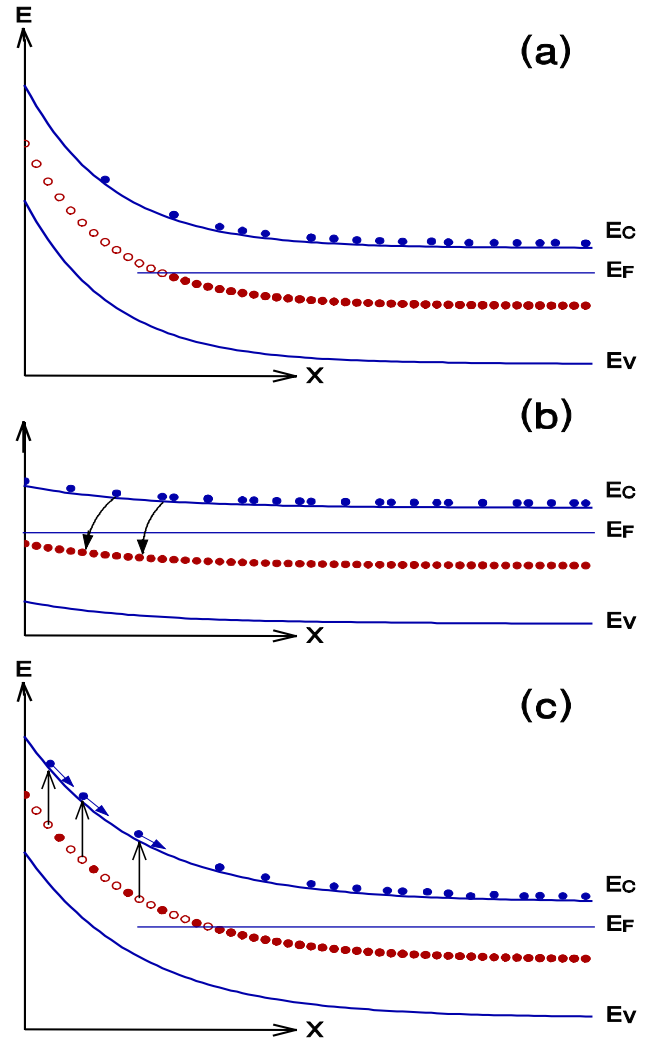
3.3 TRANSIENT CAPACITANCE SPECTROSCOPY

The general method of junction transient measurements on amorphous semiconductors has been discussed in detail in several earlier publications.[8,12,13] The basic physics of all such measurements is as shown in Fig. 1. We illustrate the situation for a semiconductor with one discrete deep gap states within the space charge region of a Schottky barrier which is subjected to a voltage "filling pulse". This pulse causes a non-equilibrium (filled) occupation of gap state to be established. As time progresses, the initial steady-state population is recovered through the excitation of trapped electrons to the conduction band where they can then move out of the depletion region under the influence of the electric field. In the dark this process proceeds entirely by the thermal excitation of trapped carriers. However, this process can be enhanced through optical excitation which is the basis of the photocapacitance and junction photocurrent techniques described Section 3.4 below.

The re-equilibration can be observed by the redistribution of trapped carriers, either as a change in the *junction capacitance* (which occurs because the depletion region will contract as negative charge is lost and the positive charge density increases) or by monitoring the *current*

which results from the motion of this charge. However, the observation of capacitance transients has one significant difference compared to current transient measurements: The dominant type

FIG. 1. Schematic diagram indicating the basic sequence of events in semiconducting junction transient measurements: **(a)** Junction under reverse bias in quasi-equilibrium showing the electronic occupation of gap states (solid circles) plus empty gap states above E_F in deep depletion (open circles). **(b)** During voltage "filling pulse" gap states capture electrons from the conduction band. **(c)** Reverse bias is restored and occupied gap states above E_F are slowly released to the conduction band due to thermal or optical excitation processes.



of emitted carrier (electron or hole) can be identified by the *sign* of the observed change in capacitance.

3.4 TRANSIENT PHOTOCAPACITANCE AND PHOTOCURRENT

The methods of junction transient photocapacitance and photocurrent have been discussed by us in great detail recently in the literature [14,15,16] and also in previous NREL reports. They represent types of sub-band-gap optical spectroscopy and provide spectra quite similar in appearance to PDS derived sub-band-gap optical absorption spectra or to spectra taken using the constant-photocurrent method (CPM). Instead of detecting absorbed energy, however, our photocapacitance and photocurrent transient methods detect the optically induced change in

defect charge within the depletion region. However, unlike the CPM method, both of our junction based techniques are not greatly influence by the free carrier mobilities since, once an electron (or hole) is optically excited into the conduction (valence) band it will either totally escape the depletion region on the timescale of our measurement (0.1 to 1s) or be retrapped into a deep state and not escape. We assume that almost all of the optically excited majority carriers (electrons) *do* escape but, in general, only a fraction of the minority carriers (holes).

Because the photocapacitance and photocurrent measurements have different sensitivities to the loss of electrons *vs.* holes from the depletion region, a detailed comparison of the two kinds of spectra can be used to disclose the escape length of the holes.[14,17] This allows us to estimate the hole $\mu\tau$ products for these samples. In these experiments the parameter τ is identified as a deep trapping time, *not* a recombination time. We are also able to distinguish whether optical excitation of defect states comes about because of the excitation of trapped electrons to the conduction band or because of the excitation of valence band electrons into an empty mobility gap state. This ability to distinguish electron from hole processes is unique among all the various types of sub-band-gap optical spectroscopies.

4.0 LIGHT INDUCED DEGRADATION KINETICS IN MIXED PHASE SAMPLES

4.1 EVIDENCE FOR PRESENCE OF MICROCRYSTALLINE COMPONENT

In this part of our work we have studied the degradation kinetics of a-Si:H films grown by dc reactive magnetron sputtering (See Section 2.1). In a previous study we showed that such films include a considerable density of microcrystallites embedded in the amorphous matrix. Evidence for the existence of these microcrystallites in these sputtered samples was first found by Raman spectroscopy.[4] Figure 2 displays a typical Raman spectrum for the sputtered samples used in this part of our study. In this case the crystalline component is clearly discernible and indicates a volume crystalline fraction of roughly 5%. Additional evidence was subsequently obtained using plan-view TEM, which was carried out by Ian Robertson's group at the University of Illinois.[18]

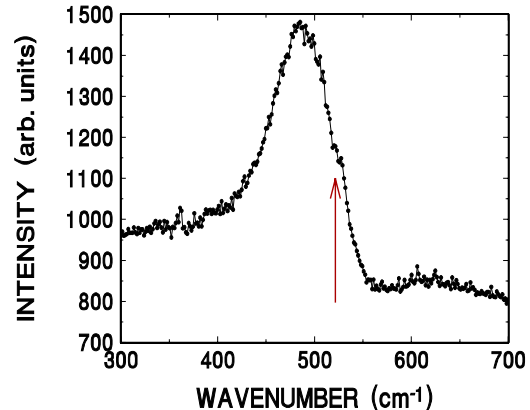


FIG. 2. Raman spectrum for Illinois, dc sputtered sample, (sample 1937) indicating a microcrystalline component at 522 cm^{-1}

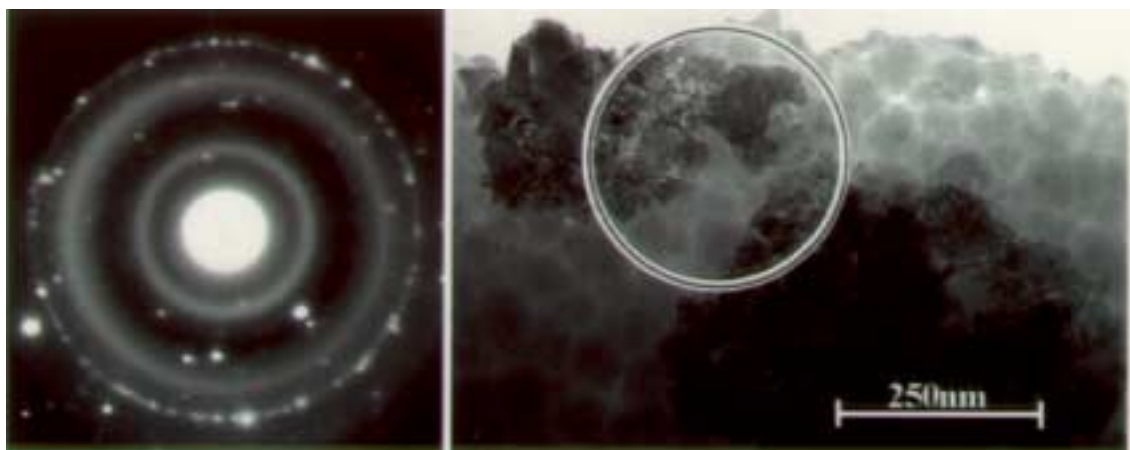
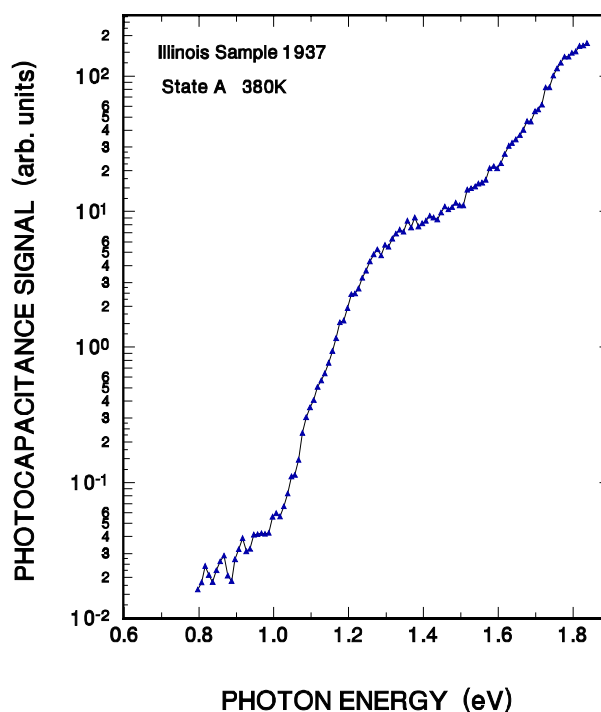


FIG. 3. Bright-field TEM image of Illinois sample 1921 taken from ref. 18. The diffraction pattern from the region circled indicates that the dark regions in the micrograph consist of fine-grained crystalline Si material.

An example of the film structure is shown in the bright-field image presented in Fig. 3. A selected area diffraction pattern from the region indicated by the circle confirms that the dark regions are actually composed of small crystallites, which give rise to the ring pattern. Dark-field microscopy using a portion of a ring confirmed that small crystallites had agglomerated to form the dark regions shown in Fig. 3. Such images indicate that these films consisted of 5 to 50 nm sized Si crystallites embedded in the amorphous silicon.

FIG. 4. Photocapacitance spectrum of Illinois sample 1937 showing a “crystalline silicon” feature with an onset close to 1.1 eV. The measurement frequency was 1kHz.



An additional and quite sensitive indicator of the presence of microcrystallites in such samples is also obtained from transient photocapacitance spectroscopy (see Section 3.4). In Fig. 4 we display the photocapacitance spectrum for the sample whose Raman spectrum is shown in Fig. 2. While the Raman evidence for the microcrystalline component in this sample is fairly subtle, the photocapacitance spectra displays a very distinct shoulder in the energy regime between 1.1 and 1.5eV. No such feature has ever been observed for standard glow discharge a-Si:H. Although we have some additional evidence that the strength of this feature scales with the strength of the corresponding Raman crystalline peak [4], the details of such a quantitative analysis are still under investigation. Nevertheless, short of carrying out TEM, we believe that the photocapacitance sub-band-gap spectra may actually provide us with our most sensitive test of the presence of a microcrystalline component in such mixed phase samples. Some of these issues are discussed further in Section 5.

4.2 BEHAVIOR OF LIGHT INDUCED DEFECT CREATION

In this Section, we demonstrate experimentally that the presence of these microcrystallites gives rise to a very unusual defect creation kinetics. The defect density in each film was determined using the drive-level capacitance profiling (DLCP) method (see Section 3.2), and the Fermi level position was determined through admittance spectroscopy (see Section 3.1). We characterized these samples following periods of light soaking using a tungsten-halogen lamp with a maximal intensity of 4.5 W/cm^2 . During light soaking the samples were immersed in methanol, to eliminate any significant increase in surface temperature. The junction capacitance measurements in every case were carried out at temperatures only up to 350K, to avoid thermal annealing of the metastable defects.

In Fig. 5 we present the results of the DLCP for one sample in various stages of light soaking (from 1 minute to 50 hours). One can see that the profiles obtained are uniform within the experimental accuracy, indicating that the material's properties are independent of the distance from the substrate. To further verify this, we repeated the experiment using the front Schottky diode, and obtained similar results. This figure reveals the unusual degradation kinetics of these a-Si:H films which is made more clear in Fig. 5(b) which presents the spatially averaged defect densities of Fig. 5(a) plotted against the light exposure time. One sees that the defect density increases significantly during the first minute of degradation, and then very slowly until 10 minutes (hereafter called "stage 1"). At this point the defect density increases dramatically in the next time interval (stage 2), and later at a more moderate pace (stage 3) followed by saturation (stage 4). All these results, including the abrupt increase in stage 2, are reproducible and independent of the specific Pd contact used.

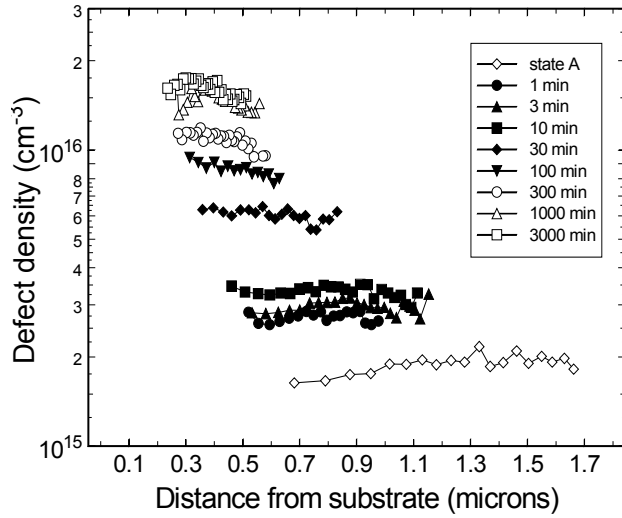


FIG. 5(a). Drive-level capacitance profiles obtained at various stages of light soaking with an intensity of 4.5 W/cm^2 . The measurements were carried out at 350K at a frequency of 11 Hz, using the substrate, p^+n , junction.

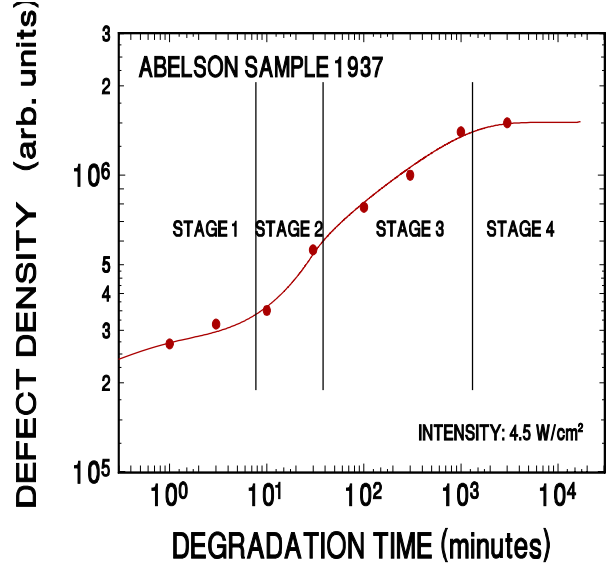


FIG. 5(b). Spatially averaged defect densities vs. light exposure time. The solid line is a guide to the eye. The increase in defect density with time falls into 4 distinct behavioral regimes which we call “stages”.

Since the DLCP technique measures the integrated density of states between the Fermi energy and a cut-off energy (which is 0.8 eV below the conduction band edge at the temperature and frequency of our measurements), it is important to determine the Fermi level position in the various stages of light soaking. We found that the Fermi energy did not shift during light soaking by more than 0.01 eV. Hence the changes in the measured profiles are directly indicative of the changes in the density of dangling bonds.

The degradation kinetics obtained for different light intensities are displayed in Fig. 6. Here we present the average defect densities obtained through the DLCP technique under three different intensities. We see that most of the features found for the high light intensity are present also in lower intensities. The main differences are that stage 1 becomes even slower as the light intensity decreases, while stage 2 gradually disappears. It is noteworthy that the transition point from stage 1 to stage 2 occurs at longer times and lower defect densities as the light intensity is reduced. The other differences, i.e. the lower overall defect density and the longer times required to achieve saturation under lower light intensity, are well known and generally occur for all a-Si:H samples [19,20].

We also examined the annealing kinetics of our samples. This was done by partially annealing the samples in steps of increasing temperature for 15 minutes at each temperature. In Fig. 7 we present the defect densities as a function of the annealing temperature. The simple curves indicate only a single type of annealing behavior. This indicates that the different steps in

FIG. 6. Defect density as a function of light soaking time for various light intensities. The densities were determined by averaging the drive-level profiles.

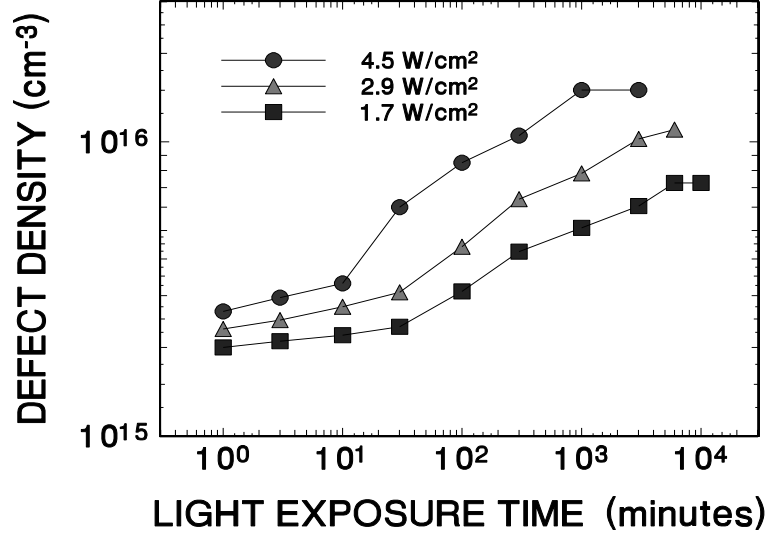
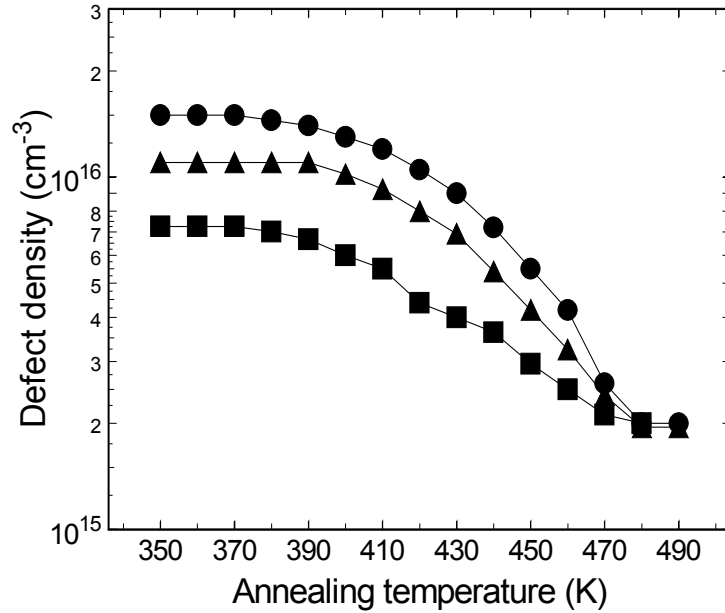


FIG. 7. The defect density as a function of the annealing temperature. These were isochronal anneals at increasing temperature of duration 15 minutes. The lines through the data are to guide the eye.



the degradation process cannot be explained by appealing to the existence of “fast” and “slow” defects as was previously proposed [21].

4.3 MODELING

The most common way to account for the degradation kinetics in a-Si:H is via the rate equation [20]:

$$\frac{dN}{dt} = \frac{C_{SW} G^2}{N^2} - \lambda f(G, N) N, \quad (4)$$

where N is the density of the dangling bond defects and G is the light intensity. The coefficients

C_{SW} and λ determine the rates of the light induced defect creation and annealing processes, respectively. We assume that light induced annealing process is initiated via the capture of one type of carrier into the metastable defects, and thus we take $f(G,N) = G/N$. This equation neglects any thermal processes, but this is a good approximation since the light soaking was carried out at temperatures which did not greatly exceed room temperature. When the light induced annealing term is negligible, the solution of the rate equation is:

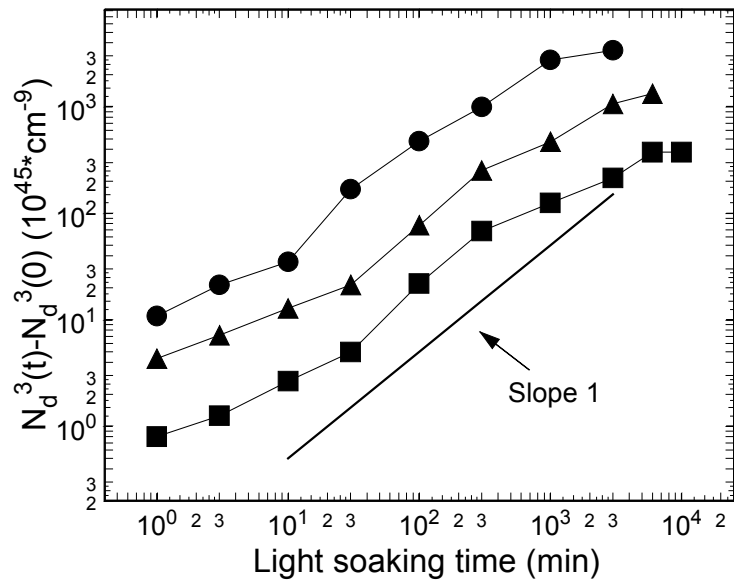
$$N^3(t) - N^3(0) = 3C_{SW} G^2 t, \quad (5)$$

so that, once the defect density significantly higher than the initial density, one obtains the well known $t^{1/3}$ rule. Indeed, a more accurate way of examining the validity of the model described by equation (4) is to plot the data according to the left hand side of equation (5), and to look for a linear relation with time. This way of presenting these data is displayed in Fig. 8. Here one can clearly see that in the short times region the experimental data definitely do *not* fit a $t^{1/3}$ dependence.

Thus stage 1 indeed represents an anomalously slow degradation not merely been masked by a high initial defect density. This means that the unusual degradation kinetics found here for amorphous silicon samples that contain microcrystallites cannot be fully accounted for by the usual kinetics of degradation even if we add in a constant component of non-degrading states associated with the microcrystallites. On the other hand, the later time regimes denoted above as stages 3 and 4 are reasonably consistent with the model represented by equation (4).

We therefore suggest that the simplest model that can account for the entire degradation kinetics is of a material which contains three phases. The first phase is high quality amorphous silicon. The second phase is a more disordered type of a-Si:H, believed to lie adjacent to the

FIG. 8. The third power of the defect density as a function of light soaking time. We have subtracted the contribution of the defects in State A. By comparing the experimental results with a line of slope 1, one can clearly see that the results follow a linear fit only in stage 3 of the degradation.



microcrystallites. The higher degree of disorder of this second phase might be due either to extra stress caused by the presence of the microcrystallites, or to a deficit of diffusing hydrogen which is able to passivate a larger fraction of the bulk defect states. The third phase are the microcrystallites, which provide only a constant, non-degrading, contribution to the defect density. In actual practice, however, we have found that this last contribution to the total defect density can be neglected. The total defect density will thus be given by $f_1 N_1 + f_2 N_2$ where N_i and f_i are the defect density and the effective volume fraction of the i^{th} phase, respectively. Since the second phase is assumed to be much more defective we start with $N_2 \gg N_1$, but we also know that $f_2 \ll f_1$. That is, the Raman spectra and TEM micrographs indicate that the vast majority of the film consists of high quality amorphous silicon.

Turning to the degradation kinetics, we assume that N_2 degrades like equation (4). However, due to the high initial defect density of this phase, the light induced annealing term in this equation will be significant even for short light soaking times. Furthermore, because this phase is highly defective, the corresponding coefficients C_{SW} and λ have relatively high values. For Phase 1 we assume that initially the recombination is governed not by the dangling bonds within this phase, but by states associated with the other two phases into which the carrier can diffuse and recombine. We denote the effective density of these centers by Z so that we can represent the lifetime for the charge carriers in Phase 1 as proportional to G/Z . This means that the rate equation for the degradation of Phase 1 in the early time regime will read:

$$\frac{d N_1}{dt} = \frac{C_{SW}^* G^2}{Z^2} - \lambda^* \frac{G}{Z} N_1 \quad (6)$$

where C_{SW}^* and λ^* denote the light induced defect creation and annealing coefficients for this phase. Note that the value of Z will depend on the light intensity used in the degradation because the position of the quasi Fermi level will alter the proportion of such states that are acting as recombination centers.

As the dangling bond density begins to increase, it will shift the quasi Fermi level towards midgap, but will not initially alter the free carrier lifetime since the collapse of the quasi Fermi level will simply deactivate an equal number of the Z states. However, once the density of the dangling bonds is high enough to deactivate *all* of the Z states the recombination kinetics will become “normal” again:

$$\frac{d N_1}{dt} = \frac{C_{SW}^* G^2}{N_1^2} - \lambda^* \frac{G}{N_1} N_1 \quad (7)$$

We note that equation (6) leads to a relatively fast initial degradation of Phase 1, one which is *linear* with time. On the other hand, once the N_1 deep defects dominate the overall recombination the degradation will follow the “normal” $t^{1/3}$ rule.

In Fig. 9 the fit lines indicate that this model can indeed account for all the features of our data. In the first stage of degradation, because the overall defect density is controlled by the contribution of Phase 2 which is high, the light induced annealing term makes the degradation kinetics slower than usual. Then, as the 1st phase defect density starts to grow (initially linearly in time) the total grows very rapidly. Shortly thereafter, this phase totally dominates the carrier recombination processes so that the degradation kinetics is controlled by the defects in this phase. The defect density dependence then rolls over into the “normal” $t^{1/3}$ behavior and ultimately saturates.

Although it may seem that this model contains a large number of free parameters, the only change we have made to between the fits for the different light intensities shown in Fig. 9(a) was in the density parameter Z . (We also change the value of G to match the experimental light intensities). This analysis indicates that Phase 1 accounts for 95% of the total and Phase 2 to only 5%. For Phase I we found fairly typical values of $C_{sw}^* = 0.0013 \text{ cm}^{-3}\text{sec}$ and $\lambda^* = 3 \cdot 10^{-13}$, while the corresponding values for the defective second phase were determined to be about 1000 times higher.

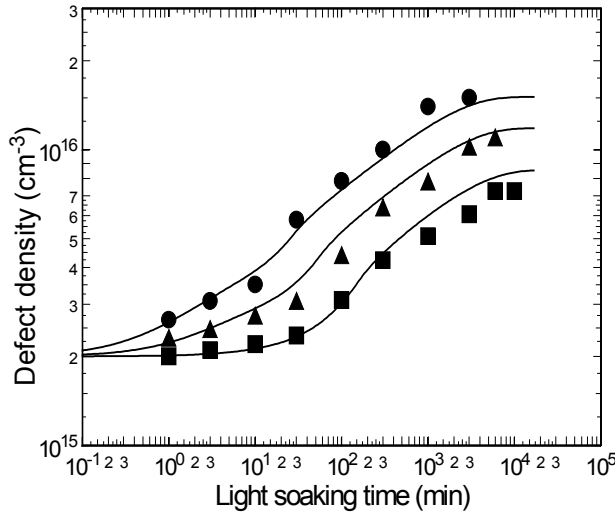


FIG. 9(a). Defect density vs. light soaking time: experiment and model. For these fits the only parameter adjusted to match the data for the different light exposure intensities was the Z concentration.

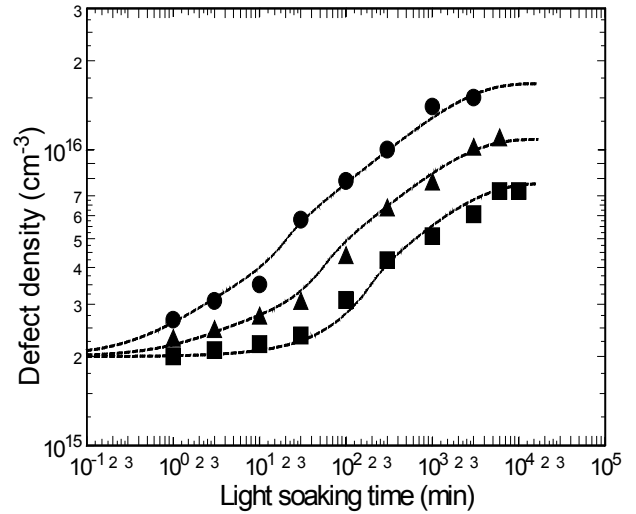


FIG. 9(b). Defect density vs. light soaking time: experiment and model. These somewhat better fits also allowed the creation coefficient C_{sw}^* to become slightly intensity dependent.

While the above fits to the experimental data are quite satisfactory, we also see that the dependence of the saturated defect density on the light intensity of these fits is not as strong as in the experiment. We can improve this if we allow C^* to be slightly dependent on G . In this case we obtain the superior fits indicated by the curves in Fig. 9(b). These fits indicate that C^* increased by 40% as the light intensity was changed by a factor of 2.8. Such a variation in the creation coefficient C^* might be explained by the existence of potential fluctuations in the Phase 1 such that a larger generation rate would allow the photocarriers to overcome these fluctuations, leading to an increase in the bi-molecular recombination rate.

More of the details of the modeling have recently been reported elsewhere [22]. We stress that the special kinetics reported here is not limited to sputtered a-Si:H samples. We have recently observed similar kinetics in some glow discharge a-Si:H samples grown under H dilution [23]. An unusually slow degradation in H diluted material has also been previously reported based on studies using the CPM technique [24]. This argues against the possibility that the results reported here are due to peculiar aspects of the DLCP technique. Indeed, it is now well known [6] that one of the effects of such dilution is the introduction of a small fraction of microcrystallites into the amorphous silicon matrix.

5.0 DEFECT BEHAVIOR OF a-Si:H NEAR THE MICROCRYSTALLINE ONSET

During the past year we have participated in a joint collaboration with researchers at Uni-Solar and at Colorado School of Mines to examine the properties of a-Si:H films grown under hydrogen dilution close to the onset of microcrystallinity. Uni-Solar provided hydrogen diluted samples of several thickness' (0.5, 1.5, and 2.5 μm on n^+ a-Si:H coated stainless steel) to Don Williamson for X-ray analysis. They also provided him with 0.5 μm thick films on 3 types of substrates (bare stainless, n^+ a-Si:H coated stainless steel, and n^+ $\mu\text{c-Si}$ coated stainless steel). They provided my group with two hydrogen diluted a-Si:H films of thickness' 1.05 and 1.3 μm on n^+ a-Si:H coated stainless steel, plus one undiluted (standard glow discharge) a-Si:H on n^+ a-Si:H coated stainless steel. For all samples we evaporated a semi-transparent Pd contact onto the top surface to produce a Schottky barrier for our junction measurements.

For the samples deposited on n^+ a-Si:H coated stainless steel, Don Williamson's X-ray analysis indicated that the films were purely amorphous at 0.5 μm thick, were mixed microcrystalline/amorphous for the 1.5 μm thick film, and were largely microcrystalline at 2.5 μm . The implication of his results was that the hydrogen diluted a-Si:H was approaching the onset of crystallinity as the film got thicker, and that the onset of distinct crystallinity occurred somewhere in excess of 1 μm .

The role of my laboratory was to assess whether the electronic properties of these films were also varying as these hydrogen diluted films increased in thickness. Scientists at Uni-Solar and ECD had reported that a-Si:H films grown under hydrogen dilution close to the onset of microcrystallinity exhibited a higher degree of stability [25]. Therefore, it seemed possible that the density of deep defects in the light-degraded state of these films would become lower as these films became thicker, at least until the onset of microcrystalline was reached.

The three films (one non H-diluted “standard” sample, plus two deposited with hydrogen dilution with different total thickness’) were characterized in a light-degraded state produced by exposure to red-filtered light from a tungsten-halogen source at an intensity of $2\text{W}/\text{cm}^2$ for 100 hours. The samples were immersed in methanol during light soaking to maintain a low surface temperature. Figure 10 displays a series of drive-level capacitance profiling (DLCP) data for the standard sample. Each profile was obtained using a measurement frequency of 33Hz and measurement temperatures were varied between 330K to 370K. Based upon cross correlation studies between ESR and DLCP on previous samples [11], we believe that a good estimate of the total defect density will be obtained by doubling the profile values displayed for the 370K curve. That is, this standard glow discharge sample has a defect density near $2 \times 10^{16} \text{ cm}^{-3}$ in its light degraded state.

Figure 11 shows the DLCP profiles at different measurement temperatures obtained for the two a-Si:H grown with hydrogen dilution (in the light degraded state). Note that the profiles for the two samples of different thickness’ are nearly identical except for the lowest temperatures where the profile distances approach the edge of the thinner sample. Also note that the higher temperature profiles exhibit considerable spatial variation, and also a defect density considerably smaller than indicated by the standard sample data, lying between 1.2 to $1.5 \times 10^{16} \text{ cm}^{-3}$.

FIG. 10. Drive-level capacitance profiles for the Uni-Solar standard glow discharge sample in its light degraded state obtained using a measurement frequency of 33Hz and several measurement temperatures. Note that the defect density profiles show very little spatial variation.

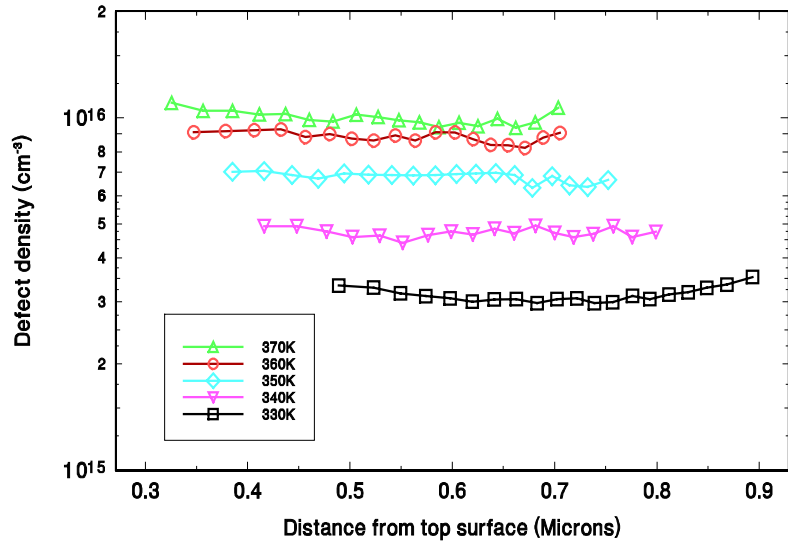


FIG. 11. Drive-level capacitance profiles for the two hydrogen diluted Uni-Solar standard glow discharge samples in their light degraded state at several measurement temperatures. Note that the profiles show considerably more spatial variation than those of the standard sample.

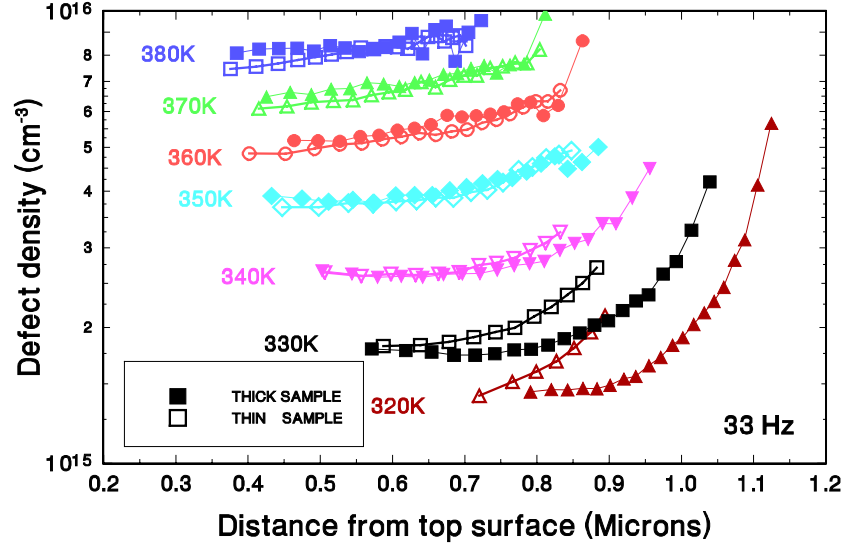
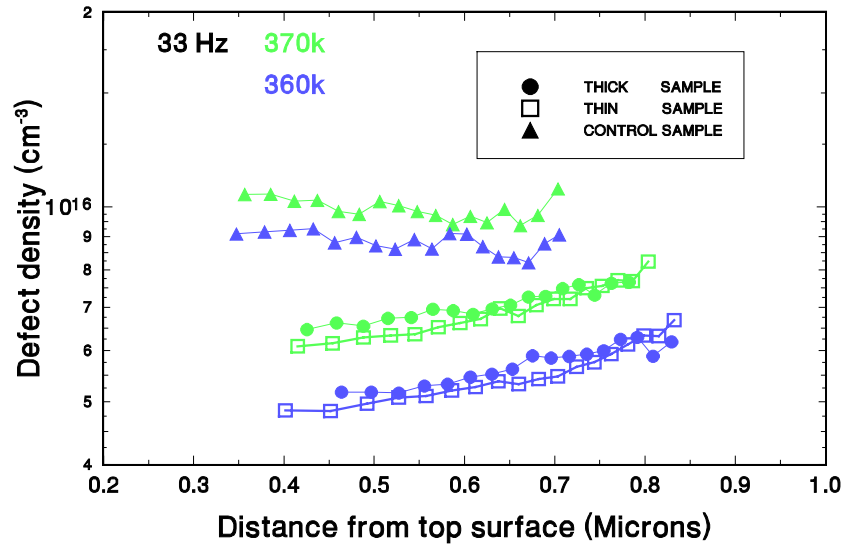


FIG. 12. Comparison of drive-level profiles for all three samples at the highest profiling temperatures. The total defect density in each film is estimated to be twice the value shown for the 370K curves in each case. Note that the profiles for the hydrogen diluted samples are significantly lower than for the standard sample and also indicate a much greater spatial variation.

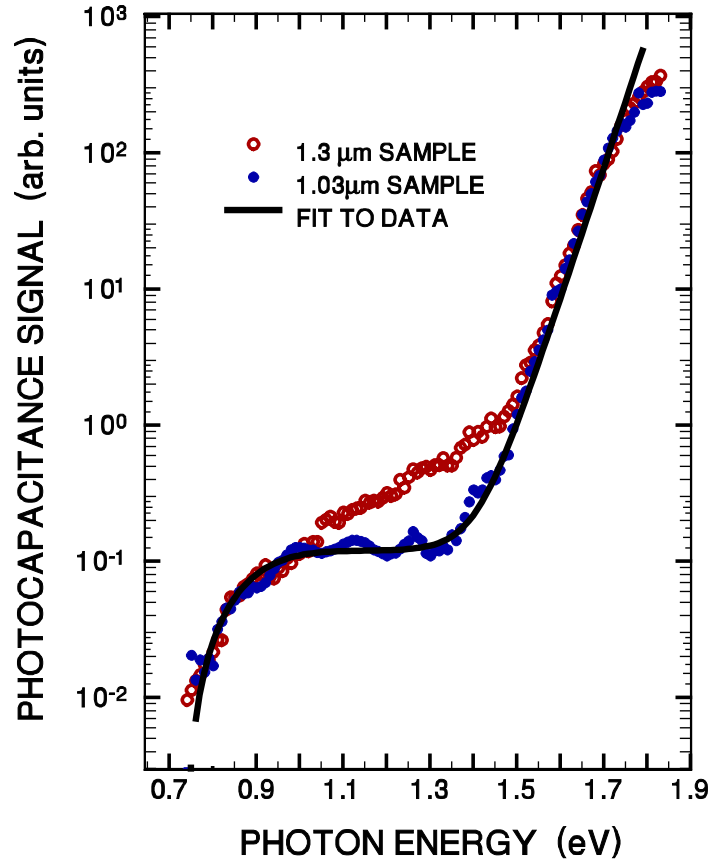


In Figure 12 we display a direct comparison between the profiles for all three samples. These are shown for the two highest measurement temperatures where the profiles should be encompassing a larger part of the deep defect band. We see that the hydrogen diluted samples exhibit defect densities roughly a factor of 1.5 lower than the standard sample, and we also note the much stronger spatial variation of the profiles for the hydrogen diluted samples. This variation indicates a decrease in deep defect density toward the top surface of those films. That is, the density of light-induced deep defects becomes smaller as we move toward the onset of microcrystallinity as deduced from the X-ray studies of Don Williamson on Uni-Solar samples deposited under the identical conditions. This tends to support the conclusion that it is this approach to microcrystallinity which leads to a more stable a-Si:H material evidenced, in this case, by a lower defect density.

Finally, in Figure 13, we display phot capacitance spectra taken for the two hydrogen diluted samples. The spectrum for the thinner sample is nearly identical to those of very high quality glow discharge samples reported previously [17,26]. The fit curve indicates an Urbach energy of 46meV. The thicker sample spectrum matches that of the thinner sample in both the bandtail regime and also at optical energies below 1.0eV where the signal is believed to originate solely from dangling bond defects in a-Si:H. However, the thicker sample has an additional feature at intermediate optical energies which, as we discussed in Section 4.1, indicates the presence of silicon microcrystallites. We believe that the volume fraction is very low for this sample, 1% or less. Indeed, such samples in our experience would not exhibit any evidence for crystallinity in Raman spectroscopy. However, our results *are* consistent with Don Williamson's X-ray results that indicate a small degree of microcrystallinity for the 1.5 μ m thick samples grown in this fashion.

Finally, matched p-i-n devices were fabricated and tested by researchers at Uni-Solar. They found a trend toward increasing open circuit voltage, V_{OC} , as the onset to crystallite formation was approached, and then an abrupt decrease in V_{OC} once this onset was exceeded.

FIG. 13. Photocapacitance spectra for the two Uni-Solar hydrogen diluted a-Si:H samples of different thickness. The thinner sample spectrum is quite similar to many published results for sub-band-gap spectra of a-Si:H in the literature. The thicker sample shows an additional feature at intermediate energies that we associate with the presence of a very small fraction of microcrystallites. The solid line is a fit to the thinner sample data which indicates an Urbach energy of 46meV and an estimated deep defect density of $1.5 \times 10^{16} \text{ cm}^{-3}$. This latter value agrees quite closely with the defect density obtained from the DLCP measurements for this sample.



6.0 CHARACTERIZATION OF HIGH GROWTH RATE a-Si:H MATERIAL

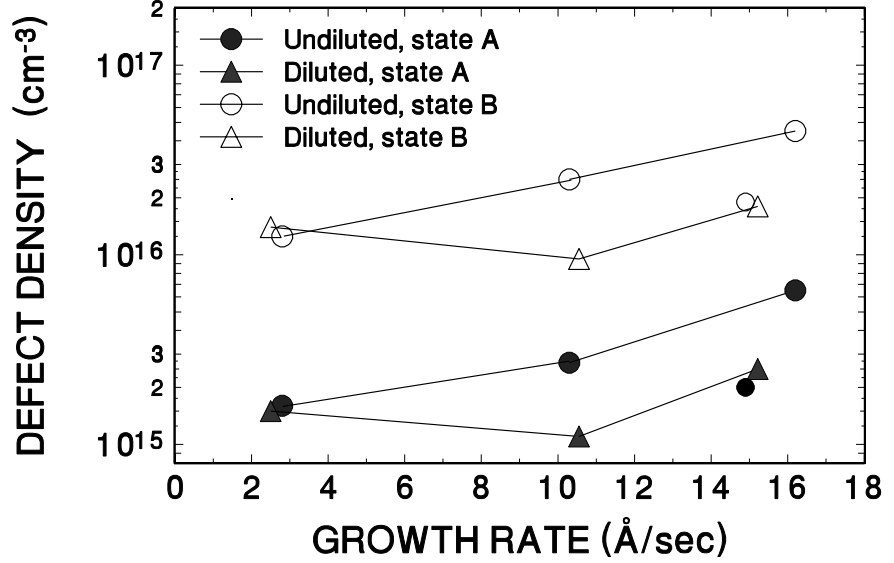
Considerable recent effort has been devoted to obtain hydrogenated amorphous silicon (a-Si:H) films that are grown at high deposition rates but contain a low defect density after light soaking. The most stable cells deposited by plasma decomposition of pure silane diluted in H_2 exhibit growth rates in the vicinity of $1\text{\AA}/\text{sec}$ which significantly limits the device fabrication rate. Thus a variety of modified deposition techniques are being explored to try to increase the growth rate while maintaining low stabilized defect densities and cell efficiencies. In this Section we report results for higher growth rate a-Si:H films obtained from two different outside laboratories: ETL and Uni-Solar.

6.1 ETL HIGH GROWTH RATE SAMPLES

We first report our results for seven samples of intrinsic a-Si:H films grown by G. Ganguly at ETL. Four of these samples were deposited without hydrogen dilution, the remaining 3 samples were diluted in hydrogen using a H_2/SiH_4 ration of 4. The rf power level was varied for each subset of samples to change the growth rate from $2.5\text{\AA}/\text{sec}$ to $15\text{\AA}/\text{sec}$. More details on the growth parameter have been presented in Section 2.2. The deep defect density in these samples was determined by the drive-level capacitance profiling (DLCP) method. We also recorded the sub-band-gap optical absorption spectra using the transient photocapacitance (TPC) technique. Films were characterized in both the dark annealed state (state A), as well as a degraded state produced by exposure to red filtered tungsten halogen light for 100 hours at an intensity of $2.2\text{ W}/\text{cm}^2$ (state B).

In Fig. 14 we plot the defect densities of these samples determined by the DLCP technique, as a function of their growth rate. Closed symbols represent the hydrogen diluted samples whereas the open symbols are for the samples grown from pure silane. For the non-diluted samples one observes that the defect density decreases as the growth rate decreases. However, for the samples grown using hydrogen dilution the defect density exhibits a shallow minimum at the relatively high growth rate of $10.5\text{ \AA}/\text{sec}$. These trends appear both in state A and state B. Furthermore, the hydrogen dilution leads to significantly lower defect densities for the samples grown at the higher rates. At the highest growth rate one obtains an almost identical reduction of the defect density by increasing the silane pressure instead of using the dilution with hydrogen. We note that all of the samples exhibit very low overall defect densities. Indeed, the extremely low defect density exhibited by the hydrogen diluted sample deposited at $10\text{ \AA}/\text{sec}$ represents *the lowest defect density we have ever recorded* for an a-Si:H film using the DLCP method.

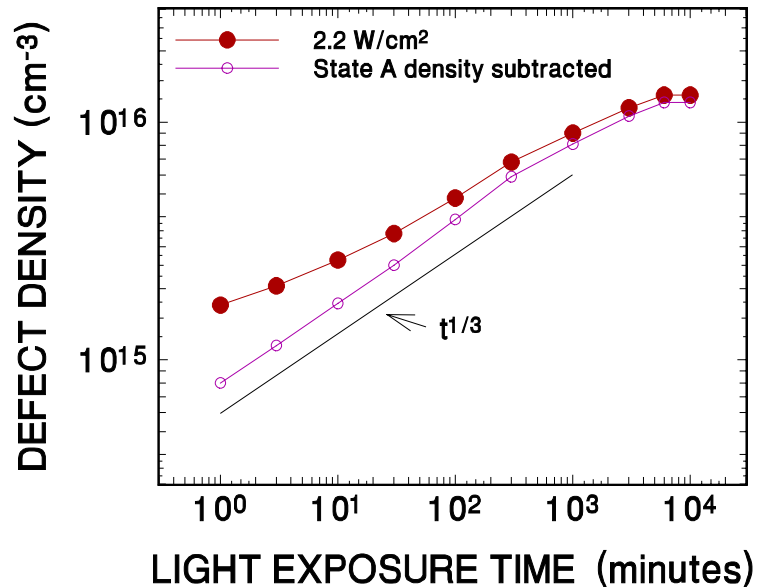
FIG. 14. Deep defect density for the ETL a-Si:H films in both their dark annealed state A, and a light degraded state B. In this case the defect densities shown are twice the drive-level densities obtained at 360K and 11Hz. Note that the undiluted film deposited at higher SiH_4 pressure (small circles) closely matches the diluted sample data for the same total chamber pressure.



We also studied the detailed degradation kinetics versus light exposure time for several of these samples. In Fig. 15 we display the results for sample 12468: that grown at a power level of 20 Watts under hydrogen dilution. These results indicate that, apart from the very low level of degradation, there is nothing unusual about the degradation kinetics compared to standard glow discharge a-Si:H samples. That is, a nearly perfect $t^{1/3}$ bimolecular dependence on light exposure time is clearly evident once the annealed (state A) deep defect density has been subtracted.

On the other hand, the sub-band-gap spectrum for this sample, displayed in Fig. 16, indicates a small component of Si microcrystallites (see Section 4.1 above). This is consistent with previous studies indicating that the most stable a-Si:H films grown under hydrogen dilution contain a small microcrystalline component. However, in contrast to the Illinois sputtered

FIG. 15. Deep defect density vs. light exposure (using an intensity of 2.2 W/cm^2) for a-Si:H sample 12468 grown under hydrogen dilution. If we subtract the defect density in state A, the defect density exhibits a nearly perfect $t^{1/3}$ dependence on exposure time.



samples (Section 4.2), this crystalline component does not give rise to any unusual degradation kinetics. This seems to indicate crystallites that have a markedly different size distribution or morphology.

The degree of microcrystallinity indicated by the sub-band-gap spectra for all of the samples in this series deposited under hydrogen dilution appear very similar to that shown in Fig. 16. However, in Fig. 17 we compare the sub-band-gap spectra for the series of the 3 *undiluted* films deposited under a 20 mTorr chamber pressure. Here we observe a systematic apparent increase in the microcrystalline “shoulder” as the growth rate is decreased from 16 Å/sec to 2.8 Å/sec.

We conclude this Section by briefly consider the how the varying growth conditions of these ETL samples may be affecting the degree of microcrystallinity. It has been argued that the formation of microcrystallites depends on the ratio of H atoms to SiH₃ radicals, with higher values promoting the formation of microcrystallites [27]. Hydrogen atoms, which originate from the dissociation of the silane molecules, collide and react with other silane molecules. This leads to the formation of more SiH₃ radicals accompanied by H₂ molecules [28]. Accordingly, at low

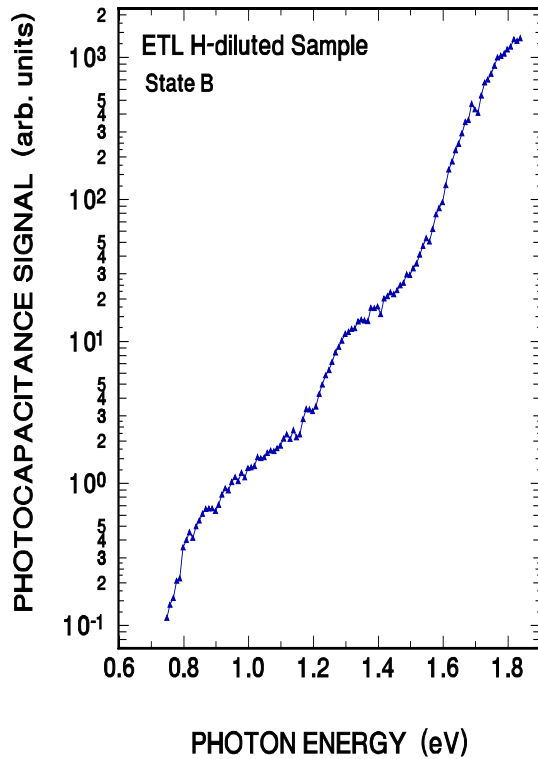


FIG. 16. Sub-band-gap, photocapacitance spectrum of the hydrogen diluted sample 12468 showing a feature with an onset close to 1.1 eV believed to be due to a small component of silicon microcrystallites.

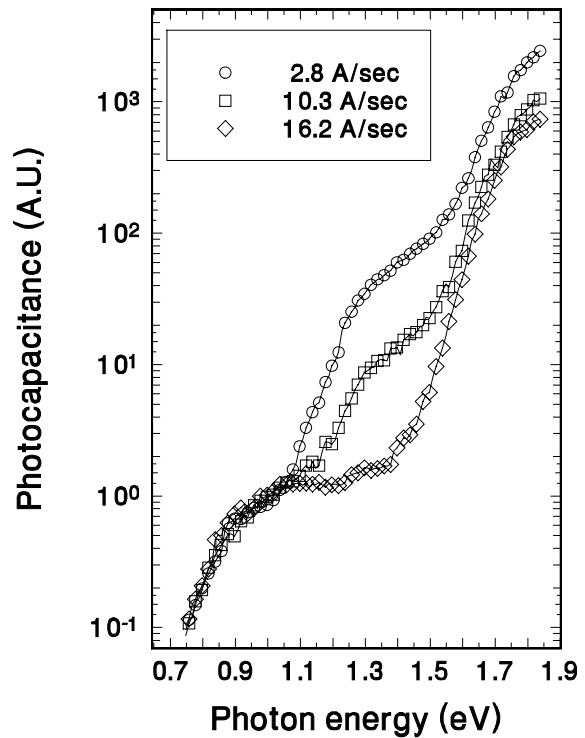


FIG 17. Photocapacitance spectra for the ETL non diluted samples. The data is for all samples in state B, and was recorded at 380K. The microcrystalline shoulder is observed to increase as the growth rate is decreased.

silane partial pressures the ratio of H/SiH₃ is high and the formation of microcrystallites is promoted. When the power is increased, H-ion bombardment energies increase and inhibit the growth of microcrystallites [27]. When H₂ is added while maintaining a low silane partial pressure, additional H atoms are formed from the dissociation of H₂ which itself does not react with H atoms, and results in higher H/SiH₃ ratios. This is reflected in the higher microcrystalline inclusion in the diluted samples.

6.2 UNI-SOLAR HIGH DEPOSITION RATE a-Si:H FILMS

A preliminary series of three a-Si:H samples was obtained from Uni-Solar. In contrast to the ETL material discussed in Section 6.2, these 3 films had been optimized at their respective growth rates in terms of delivering good performance for photovoltaic p-i-n cells. One film was low growth rate hydrogen diluted material deposited at 1Å/sec. This corresponds to the material that has produced the most stable, highest efficiency devices produced at Uni-Solar. The other two samples were deposited at 3Å/sec and 6Å/sec. The first of these was deposited in a conventional PECVD reactor utilizing modified deposition conditions (higher rf power, etc.), while the second was deposited under VHF conditions using a 70 MHz excitation frequency. Both films were deposited under conditions that have led to the best performing cells reported to date for these higher deposition rates.

Each film was deposited on a stainless steel substrate over a thin contacting layer of n⁺ a-Si:H. A Pd Schottky contact was deposited onto the top surface of each sample to enable characterization by our junction capacitance methods. Capacitance vs. frequency and temperature allowed us to determine the thickness of each sample as well as the activation energy of the dark conductivity, E_σ. These quantities are listed in Table II.

We then carried out drive-level capacitance profiling (DLCP) measurements to assess overall defect density and spatial uniformity of electronic properties. We also carried out transient photocapacitance (TPC) spectroscopy, to document the sub-band-gap spectra and thus, for example, document differences in the Urbach energies or deep defect energy distributions. The above measurements were all carried out for the light-degraded state of these sample which were obtained by an exposure to a red filtered tungsten-halogen source at an intensity of 2W/cm² for 100 hours. These defect densities and Urbach energies have been included in Table II.

A comparison of the drive-level capacitance profiles for all 3 samples in their light-degraded state is shown in Fig. 18. At the measurement frequency and temperature employed, the deep

TABLE II. Properties deduced for Uni-Solar a-Si:H samples of varying deposition rate. All three samples were deposited on n+ a-Si:H coated stainless steel substrates. The thickness and activation energy of conductivity were determined from admittance vs. temperature and frequency measurements, the Urbach energies were determined from the transient photocapacitance spectra (see Fig. 19), and the deep defect densities were determined from the drive-level capacitance profiling measurements (see Fig. 18).

SAMPLE	Deposition Rate	Thickness	Conductivity Activation Energy (eV)	Urbach Energy (meV)	Deep Defect Density (cm^{-3})
10065	1 Å/sec	1.05 μm	0.73	46	1.5×10^{16}
B4345	3 Å/sec	1.2 μm	0.77	45	2.5×10^{16}
R7625	6 Å/sec	1.05 μm	0.73	48	3.5×10^{16}

defect density is approximately twice the density given on the vertical axis. One notes that the deep defect density increases markedly as the deposition rate increases, and also that its spatial variation becomes somewhat larger. The sub-band-gap spectra for these three films obtained from the transient photocapacitance measurements are shown in Fig. 19. The three samples exhibit quite similar sub-band-gap spectra. The only significant evidence for poorer film properties at the higher deposition rate material from these spectra is a moderate increase in the deep defect density consistent with that obtained from the DLCP data, and a slightly wider Urbach tail obtained for the film deposited at 6 Å/sec.

FIG. 18. Drive-level capacitance profiles for three Uni-Solar a-Si:H samples in their light degraded states. These samples were deposited at the three different growth rates indicated using conditions which have led to the best stabilized cell performance obtained at Uni-Solar. The profiles were carried out using a measurement frequency of 33Hz and a temperature of 370K. Under such conditions the total deep defect density is approximately twice that shown on the vertical axis.

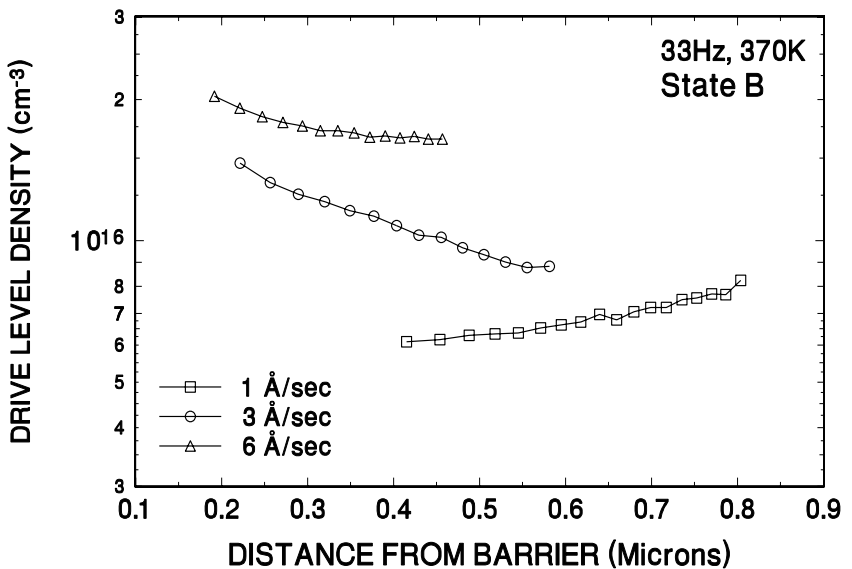
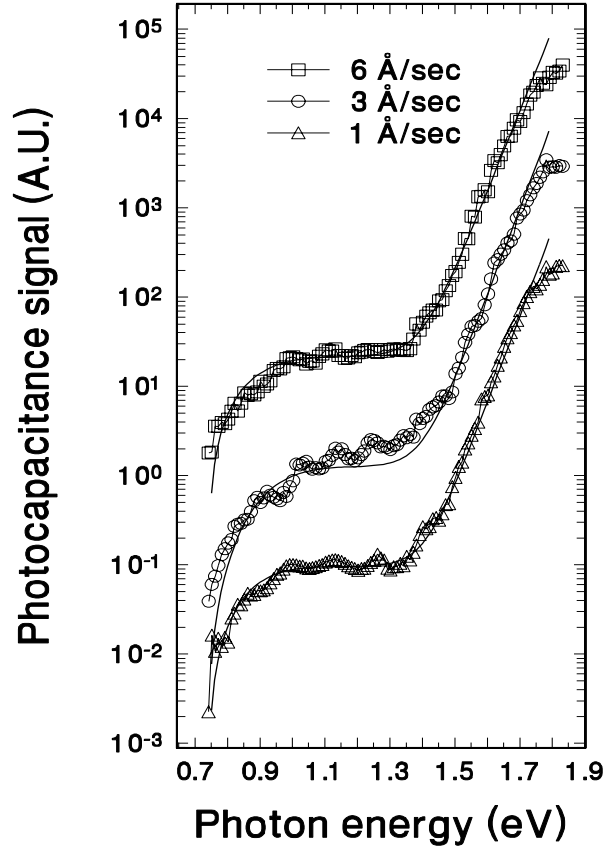


FIG. 19. Sub-band-gap spectra obtained from transient photocapacitance measurements of the three Uni-Solar samples in their light degraded state. The three spectra have been offset vertically for display purposes. The thin solid lines are fits to these spectra used to estimate the deep defect densities and to determine the value of the Urbach energies



We can formulate a few general conclusions of this quite preliminary study of the effects of increased deposition rate on the electronic properties of the Uni-Solar a-Si:H films. Specifically, our measurements do show differences in the electronic properties consistent with poorer device performance; namely, a moderate increase in deep defect density and a slight increase in the width of the Urbach tail. Unfortunately, the current samples do not yet allow us to perform measurements to assess minority carrier transport properties. We are currently planning a more comprehensive series of studies to examine such effects.

7.0 DEFECT DENSITIES IN THE AMORPHOUS SILICON-GERMANIUM ALLOYS

While, in this Subcontract period, my group did not carry out any new measurements pertaining to the low gap a-Si_{1-x}Ge_x:H alloys, we did carry out some new calculations to better understand the results we have obtained previously.

My group has been applying our experiment methods to characterize the electronic properties of a-Si_{1-x}Ge_x:H alloys since 1990. The films we studied were produced by at different laboratories using three different growth methods: Photo-CVD at IEC, Delaware; Cathodic glow discharge at Harvard; and standard glow discharge at Uni-Solar. Although some of the details in the behavior of these samples were found to be different, all of these sets of samples were found to exhibit superior properties compared to those of a-Si_{1-x}Ge_x:H alloys reported elsewhere (that is, they exhibited narrower Urbach tails and lower defect densities). To illustrate this I have compiled, in Fig. 20, the values of the Urbach energy parameter determined for these 3 sets of alloy samples together with those determined for sets of alloy samples reported previously in the literature.[29-35] One notices that, in particular, the Harvard and Uni-Solar samples exhibit Urbach energies as low as those found in pure a-Si:H, independent of the Ge content. This indeed seems to indicate that a distinct level of optimization that has now been achieved in the a-Si_{1-x}Ge_x:H alloy system. In Fig. 21 I compare deep defect levels for these three sets of alloys,

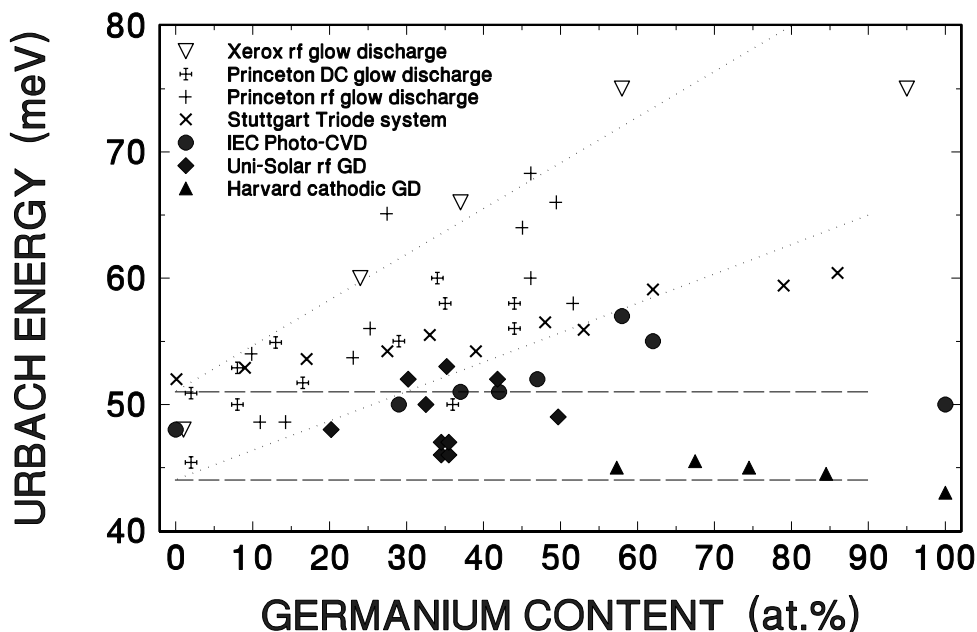


FIG. 20. Urbach energies vs. Ge content determined from sub-band-gap spectra for a-Si_{1-x}Ge_x:H samples taken from different studies. The dotted lines indicate the trend in Urbach energies from the studies carried out before 1990, while the dashed lines indicate the range of values observed in our more recent studies of IEC, Harvard, and Uni-Solar a-Si_{1-x}Ge_x:H samples.

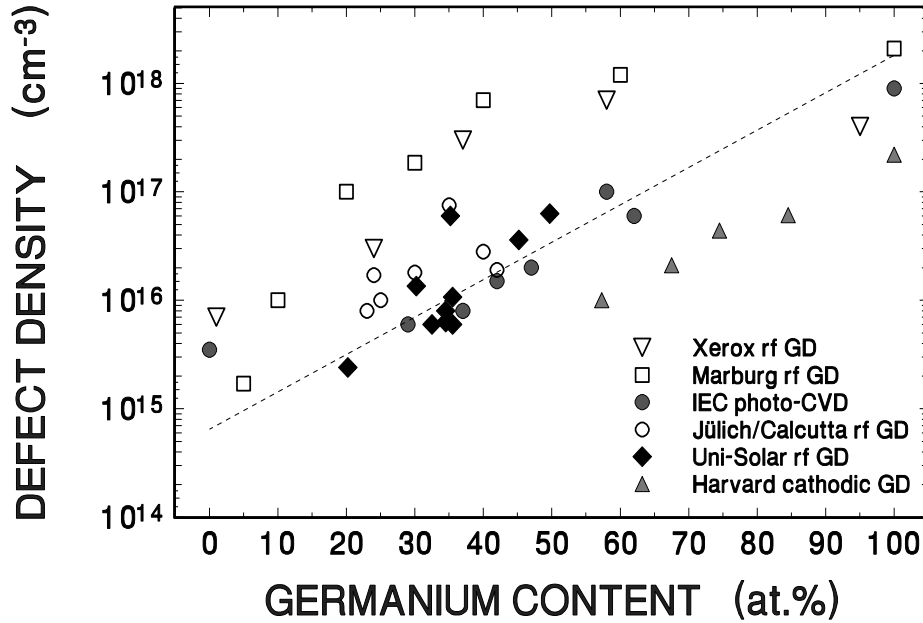
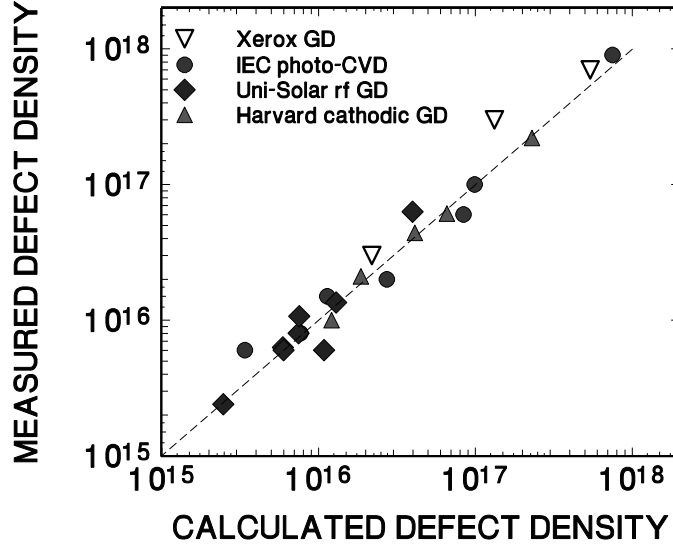


FIG. 21. Defect densities vs. Ge content determined from ESR measurements (open symbols) and capacitance profiling studies (solid symbols). The sources of these data are given in the text. The dashed line is a guide to the eye.

determined using the DLCP method [32,33,34,35], with defect level determined using ESR from other groups [30,36,37]. Other studies that estimate of defect densities from sub-band-gap optical spectra, while useful within a given series of samples, is less quantitative and so is probably not too reliable for comparison between samples from different sources. Nonetheless, defect densities estimated from optical spectra also agree quite well with the trend shown in Fig. 21, indicating an exponential increase, by roughly a factor of 300 overall, as x varies from 0 to 1.[29,38,39]

Figures 20 and 21 indicate that the 3 series of a-Si_{1-x}Ge_xH samples that my group has investigated (from U. Delaware, Harvard, and Uni-Solar) come very close to being optimized in the sense that they exhibit Urbach tail energies as low as high quality a-Si:H and also quite low deep defect levels overall. One additional indicator that these a-Si_{1-x}Ge_xH alloy samples are optimized is the degree to which they obey the spontaneous bond breaking model of M. Stutzmann [40]. This model was proposed as a simple alternative to the “defect pool” types of arguments [29,41], although it is not necessarily inconsistent with these. It was originally proposed to account for the correlation between defect densities and Urbach energies in pure a-Si:H, but it has also been found to account remarkably well for the variation of defect density with the changes in Ge fraction in the a-Si_{1-x}Ge_xH alloys [42]. It implies the simple relation:

FIG. 22. Measured defect densities vs. the value predicted from the spontaneous bond-breaking model of M. Stutzmann. The dashed line indicates perfect agreement. The data also includes an early study from the Xerox group for which the defect density values were known quantitatively from ESR and the values of the Urbach and optical gap energies were also reported.



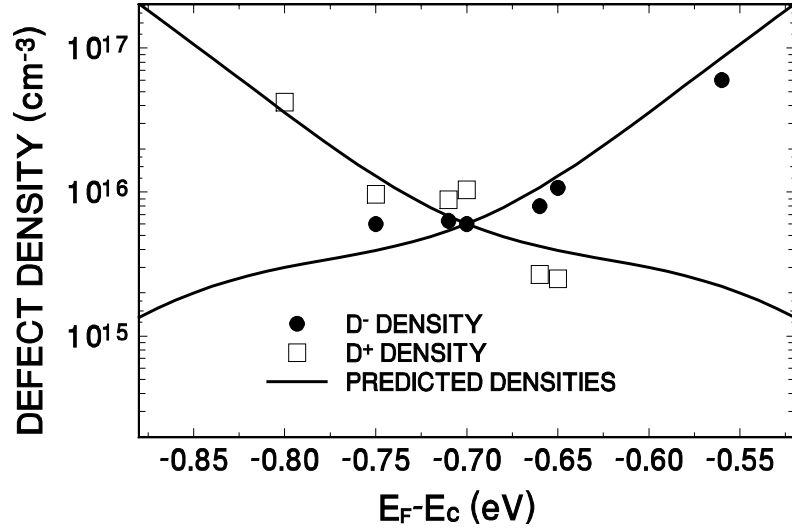
$$N_D = N_0 E_U \exp[-(E_D - E^*)/E_U] \quad (8)$$

where E_D is the energy position of the deep defect band within the gap (obtained, for example, from the sub-band-gap optical spectrum), E^* is a demarcation energy separating bandtail states from deep defects, and N_0 is the density of states close to the valence band mobility edge. In practice the parameters N_0 and E^* merely provide the freedom to adjust the overall magnitude of the deep defect density to match experiment. However, a single choice of these parameters (e.g., $N_0 = 10^{21} \text{ cm}^{-3}$, $E^* \approx E_V + 0.15 \text{ eV}$) provides very good agreement to the defect densities found by my group for all of the IEC, Harvard, and Uni-Solar samples. This is illustrated in Fig. 22.

While the spontaneous bond breaking model thus accounts quite well for the defect densities in *intrinsic* samples, it is well known that doped samples exhibit defect densities more than one order of magnitude larger without much variation in the Urbach energy or defect energy position. Clearly the simple relation of Eq. (8) does not apply to doped samples because it omits the energy gain due to charge redistribution when dopants shift the Fermi level position.

During the past year we thus attempted to construct a modified spontaneous bond breaking model that would properly take into account the changes in defect formation energy due to the variations in the position of Fermi energy that result from doping. This was also important regarding our recent conclusion that considerable concentrations of charged defects existed in the Uni-Solar a-Si,Ge:H samples.[43] Thus we wished to find out whether such a modified spontaneous bond breaking model would be consistent with the variations in positive and negatively charged defects we believed we had identified in these samples. Indeed, the series of Uni-Solar samples we had been studying included seven samples with Ge fractions near 35 at.%.

FIG. 23. Measured charged defect densities vs. the value predicted from the modified spontaneous bond-breaking model for Uni-Solar 35at.% Ge samples.



Three of these were nearly intrinsic with a conductivity activation energy near $E_g/2$, two others were *v*-type with a 50 to 100 meV lower conductivity activation energies, one was lightly *n*-type doped with a 200 meV lower conductivity activation energy, and one was lightly *p*-type doped with a 100 meV lower activation energy (but in this case because E_F is closer to the *valence* band).

One finds that for doped samples, whether the Fermi level lies closer to conduction band or to valence band, the overall total energy, E_{total} , will always be decreased relative to the intrinsic case. We can thus incorporate this additional energy gain into the spontaneous bond breaking model to predict that:

$$N_{doped} = N_{intrinsic} \exp\{-[E_{total}(E_F) - E_{total}(E_F^i)]/E_U\} \quad (9)$$

where E_F^i is the Fermi energy of the intrinsic sample, N_{doped} and $N_{intrinsic}$ are the total defect densities for doped and intrinsic samples, respectively. Also, if we know the Fermi energy position for intrinsic samples, then we can also obtain the ratios of positively, neutrally and negatively charged defects for the sample as a function of E_F . In Fig. 23 we display the predicted values we have calculated using this modified spontaneous bond breaking model and the concentration of charged defects for the $x = 0.35$ Uni-Solar a-Si_{1-x}Ge_xH alloys deduced in ref. 43. For our calculation, we used a value $E_F^i - E_c = -0.7$ eV for the Fermi energy position of the most intrinsic samples, and chose the Gaussian defect band to have a standard deviation of $\sigma = 0.07$ eV, corresponding to an average of values obtained by fitting the experimental optical spectra. We see that the agreement of this calculation to our experimentally determined defect densities is quite satisfactory. More of the details of our analysis were presented at the April 1998 MRS Meeting [44].

8.0 SUMMARY AND CONCLUSIONS

An overriding theme of the work described above in this first phase of our NREL Subcontract has been the effect of partial crystallinity, or the approach to partial crystallinity, on the electronic properties of a-Si:H. This includes, of course, how degradation or the relative stability of these films is affected by the approach to, or onset of, microcrystallinity. We first discussed the results on a set of samples produced by dc reactive magnetron sputtering, obtained in collaboration with John Abelson's group at the University of Illinois, for which we demonstrated the existence of a small but significant microcrystalline component. For these films the degradation kinetics was found to be quite unusual; however, it could be well accounted for by a model that postulated two phases of degrading material. One was a-Si:H host material of good quality and the other was a more defective component associated with boundary regions near the microcrystallites. Our sub-band-gap photocapacitance measurements on these films also indicated the existence of a distinct feature (a "shoulder" with a threshold near 1.1eV) that signaled the presence of the microcrystalline phase.

The second set of samples investigation were produced by Uni-Solar, deposited under conditions of high hydrogen dilution, very close to but just below the microcrystalline phase boundary. Here we found that the defect density following light-induced degradation decreased as the film thickness increased. Corroborating our findings with X-ray diffraction results obtained by Don Williamson on sets of similar films, we concluded that the films were becoming more ordered and less defective just prior to the onset of a detectable microcrystalline component. Furthermore we found that at almost exactly the conditions that Don Williamson found XRD evidence for the onset of microcrystallinity we found the appearance of the distinctive "shoulder" in our sub-band-gap photocapacitance spectra.

Third, we investigated two sets of samples where the deposition rate had been varied to include samples grown at moderate to high rates. In one set of samples, produced at ETL, samples deposited under H₂ dilution at 10 Å/sec were found to exhibit extremely low deep defect densities and narrow Urbach tails, indicating films of exceptional quality. The photocapacitance spectra for these films were found to contain evidence for a small degree of microcrystallinity. In another set of samples, produced at Uni-Solar, we found evidence for increasing defect densities plus somewhat larger Urbach energies for the films deposited at higher rates. This is consistent with the fact that the photovoltaic device performance is significantly poorer for the higher deposition rate material.

Finally, we discussed the general issue of deep defect densities in the a-Si_xGe_{1-x}H alloys. We again demonstrated how well the deep defect densities in such samples from several sources could be fit using the spontaneous bond-breaking model of Martin Stutzmann [40]. This implies that such state-of-the-art alloy films have been optimized in a quantifiable sense. We also found that the increase in deep defect density with small amounts of P and B dopants could also be reproduced reasonably well by modifying the spontaneous bond-breaking model to include the extra energy terms associated with charged defects.

9.0 SUBCONTRACT SUPPORTED PUBLICATIONS

1. Chih-Chiang Chen, Fan Zhong, J. David Cohen, Jeffrey C. Yang, and Subhendu Guha, "Evidence for charged defects in intrinsic glow discharge hydrogenated amorphous silicon-germanium alloys", *Phys. Rev. B* **57**, R4210 (1998).
2. Yoram Lubianiker, J. David Cohen, Hyun-Chul Jin, and John R. Abelson, "Degradation kinetics of hydrogenated amorphous silicon: the effect of embedded microcrystallites", *Mat. Res. Soc. Symp. Proc.* **507**, 729 (1998).
3. Chih-Chiang Chen, Yoram Lubianiker, J. David Cohen, Jeffrey C. Yang, Subhendu Guha, Paul Wickboldt, and William Paul, "The electronic structure, metastability, and transport properties of optimized amorphous silicon-germanium alloys", *Mat. Res. Soc. Symp. Proc.*, **507**, 769 (1998).
4. S. Guha, J. Yang, D.L. Williamson, Y. Lubianiker, J.D. Cohen, and A.H. Mahan, "Structural, defect and device behavior of hydrogenated amorphous Si near and above the onset of microcrystallinity", *Appl. Phys. Lett.* **74**, 1860 (1999).
5. Y. Lubianiker, J.D. Cohen, H-C. Jin and John R. Abelson, "The effect of embedded microcrystallites on the light - induced degradation of hydrogenated amorphous silicon", *Phys. Rev. B* **60**, 4434 (1999).

10.0 REFERENCES

1. M. Pinarbasi, M. J. Kushner, and J. R. Abelson, J. Appl. Phys. **68**, 2255 (1990).
2. G. Feng, M. Katiyar, Y. H. Yang, J. R. Abelson, and N. Maley, Mat. Res. Soc. Symp. Proc. **258**, 179 (1992).
3. J.E. Gerbi and J.R. Abelson, Mat. Res. Soc. Symp. Proc. **507**, 429 (1998).
4. D. Kwon, H. Lee, J.D. Cohen, H.-C. Jin, and J.R. Abelson, J. Non-Cryst. Solids **227-230**, 1040 (1998).
5. R. Hayashi, T. Takagi, G. Ganguly, M. Fukawa, M. Kondo and A. Matsuda, Proc. 2nd WCEPVSEC, 925 (1998).
6. J. Yang, A. Banerjee, and S. Guha, Appl. Phys. Lett. **70**, 2975 (1997).
7. S. Guha, J.S. Payson, S.C. Agarwal, and S.R. Ovshinsky, J. Non-Cryst. Solids **97-98**, 1455 (1988).
8. D.V. Lang, J.D. Cohen, and J.P. Harbison, Phys. Rev. B **25**, 5285 (1982).
9. C.E. Michelson, A.V. Gelatos, and J.D. Cohen, Appl. Phys. Lett. **47**, 412 (1985).
10. K.K. Mahavadi, K. Zellama, J.D. Cohen, and J.P. Harbison, Phys. Rev. B **35**, 7776 (1987).
11. T. Unold, J. Hautala, and J.D. Cohen, Phys. Rev. B **50**, 16985 (1994).
12. Lang, D.V. in *Thermally Stimulated Relaxation in Solids*, vol. 37 of Topics in Applied Physics, ed by P. Braunlich (Springer, Berlin, 1979), p. 93.
13. Cohen, J.D., in *Hydrogenated Amorphous Silicon*, vol. 21C of *Semiconductors and Semimetals*, ed. by J. Pankove (Academic Press, New York, 1984), p. 9.
14. J.D. Cohen and A.V. Gelatos, in *Advances in Disordered Semiconductors Vol I: Amorphous Silicon and Related Materials*, ed. by H. Fritzsche (World Scientific, Singapore, 1988), pp. 475-512.
15. J. David Cohen, Thomas Unold, A.V. Gelatos, and C.M. Fortmann, J. Non-Cryst. Solids **141**, 142 (1992).
16. T. Unold, J.D. Cohen, and C.M. Fortmann, Mat. Res. Soc. Symp. Proc. **258**, 499 (1992).
17. A.V. Gelatos, K.K. Mahavadi, and J.D. Cohen, Appl. Phys. Lett. **53**, 403 (1988).
18. D. Kwon, C.-C. Chen, J.D. Cohen, H.-C. Jin, E. Hollar, I. Robertson, and J.R. Abelson, Phys. Rev. B **60**, 4442 (1999).
19. M. Stutzmann, W.B. Jackson and C.C. Tsai, Phys. Rev. B **32**, 23 (1985).
20. Z.Y. Wu, J.M. Siefert and B. Equer, J. Non-Cryst. Solids **137-138**, 227 (1991).
21. L. Yang and L.-F. Chen, Mat. Res. Soc. Symp. Proc. **297**, 619 (1993).
22. Y. Lubianiker, J.D. Cohen, H.-C. Chul, and J.R. Abelson, Mat. Res. Soc. Symp. Proc. **507**, 729 (1998).
23. Unusual defect creation kinetics have been observed in several a-Si:H samples deposited under high hydrogen dilution by the Penn State group.
24. S. Vignoli, R. Meaudre, M. Meaudre, P. Roca I Cabarrocas, C. Godet and P. Morin, J. Non-Cryst. Solids **198-200**, 474 (1996).

25. D.V. Tsu, B.S. Cho, S.R. Ovshinsky, S. Guha and J. Yang, Appl. Phys. Lett. **71**, 1317 (1997).
26. A.V. Gelatos, K.K. Mahavadi, J.D. Cohen, and J.P. Harbison, Appl. Phys. Lett. **53**, 403 (1988).
27. A. Matsuda, J. Non-Cryst. Solids **59-60**, 767 (1983).
28. R. Robertson and A. Gallagher, J. Appl. Phys. **59**, 3402 (1986).
29. S. Aljishi, Z E. Smith, and S. Wagner, in *Amorphous Silicon and Related Materials*, ed. by H. Fritzsche (World Scientific, Sinapore, 1989), pp. 887-938.
30. M. Stutzmann., R.A. Street, C.C. Tsai, J.B. Boyce, and S.E. Ready, J. Appl. Phys. **66**, 569 (1989).
31. H.C. Weller, F. Kessler, E. Lotter, C.E. Nebel, S.M. Paasche, and G.H. Bauer, J. Non-Cryst. Solids **97&98**, 1071 (1987).
32. T. Unold, J.D. Cohen, and C.M. Fortmann, Appl. Phys. Lett. **64**, 1714 (1994).
33. F. Zhong, J.D. Cohen, J.C. Yang, and S. Guha, Mat. Res. Soc. Symp. Proc. **336**, 493 (1994).
34. J.D. Cohen, T. Unold, C.-C. Chen, and F. Zhong, unpublished.
35. F. Zhong, C.-C. C. Chen, J.D. Cohen, P. Wickboldt, and W. Paul, Mat. Res. Soc. Symp. Proc. **377**, 553 (1995).
36. W. Fuhs and F. Finger, J. Non-Cryst. Solids **114**, 1387 (1989).
37. C. Maltern, F. Finger, J. Fölsch, T. Kulesa, H. Wagner, S. Ray, A.R. Middya, and S. Hazra, Mat. Res. Soc. Symp. Proc. **377**, 559 (1995).
38. P. Della Sula, C. Reita, G. Conte, F. Galluzzi and G. Grillo, J. Appl. Phys. **67**, 814 (1990).
39. W. Paul, J.H. Chen, E.Z. Liu, A.E. Wetsel, and P. Wickboldt, J. Non-Cryst. Solids **164-166**, 1 (1993).
40. M. Stutzmann, Philos. Mag. B**60**, 531 (1989).
41. Z E. Smith and S. Wagner in *Amorphous Silicon and Related Materials* (Ref. 29), pp. 409-460.
42. T. Unold, J.D. Cohen, and C.M. Fortmann, Appl. Phys. Lett. **64**, 1714 (1994).
43. C.-C. Chen, F. Zhong, J.D. Cohen, J. Yang, and S. Guha, Phys. Rev. B**57**, R4210 (1998).
44. C.-C. Chen, Y. Lubianiker, J.D. Cohen, J.C. Yang, S. Guha, P. Wickboldt, and W. Paul, Mat. Res. Soc. Symp. Proc., **507**, 769 (1998)..

REPORT DOCUMENTATION PAGE			Form Approved OMB NO. 0704-0188	
Public reporting burden for this collection of information is estimated to average 1 hour per response, including the time for reviewing instructions, searching existing data sources, gathering and maintaining the data needed, and completing and reviewing the collection of information. Send comments regarding this burden estimate or any other aspect of this collection of information, including suggestions for reducing this burden, to Washington Headquarters Services, Directorate for Information Operations and Reports, 1215 Jefferson Davis Highway, Suite 1204, Arlington, VA 22202-4302, and to the Office of Management and Budget, Paperwork Reduction Project (0704-0188), Washington, DC 20503.				
1. AGENCY USE ONLY (Leave blank)		2. REPORT DATE March 2000		3. REPORT TYPE AND DATES COVERED Annual Subcontract Report, 16 January 1998–15 January 1999
4. TITLE AND SUBTITLE Identifying Electronic Properties Relevant to Improving the Performance and Stability of Amorphous Silicon-Based Mid-Gap and Low-Gap Cells; Annual Subcontract Report, 16 January 1998–15 January 1999			5. FUNDING NUMBERS C: XAF-8-17619-05 TA: PV005001	
6. AUTHOR(S) J.D. Cohen				
7. PERFORMING ORGANIZATION NAME(S) AND ADDRESS(ES) Department of Physics and Materials Science Institute University of Oregon Eugene, Oregon 97403			8. PERFORMING ORGANIZATION REPORT NUMBER	
9. SPONSORING/MONITORING AGENCY NAME(S) AND ADDRESS(ES) National Renewable Energy Laboratory 1617 Cole Blvd. Golden, CO 80401-3393			10. SPONSORING/MONITORING AGENCY REPORT NUMBER SR-520-28050	
11. SUPPLEMENTARY NOTES NREL Technical Monitor: B. von Roedern				
12a. DISTRIBUTION/AVAILABILITY STATEMENT National Technical Information Service U.S. Department of Commerce 5285 Port Royal Road Springfield, VA 22161			12b. DISTRIBUTION CODE	
13. ABSTRACT (<i>Maximum 200 words</i>) An overriding theme of the work described in this report has been the effect of partial crystallinity, or the approach to partial crystallinity, on the electronic properties of a-Si:H. This includes, of course, how degradation or the relative stability of these films is affected by the approach to, or onset of, microcrystallinity. We first discussed the results on a set of samples produced by dc reactive magnetron sputtering, obtained in collaboration with John Abelson's group at the University of Illinois, for which we demonstrated the existence of a small, but significant, microcrystalline component. For these films, the degradation kinetics was found to be quite unusual; however, it could be well accounted for by a model that postulated two phases of degrading material. One was a-Si:H host material of good quality and the other was a more defective component associated with boundary regions near the microcrystallites. Our sub-band-gap photocapacitance measurements on these films also indicated the existence of a distinct feature (a "shoulder" with a threshold near 1.1 eV) that signaled the presence of the microcrystalline phase. The second set of samples investigated were produced by Uni-Solar, deposited under conditions of high hydrogen dilution, very close to but just below the microcrystalline phase boundary. Here we found that the defect density following light-induced degradation decreased as the film thickness increased. Corroborating our findings with X-ray diffraction results obtained by Don Williamson on sets of similar films, we concluded that the films were becoming more ordered and less defective just prior to the onset of a detectable microcrystalline component. Furthermore, we found that at almost exactly the conditions that Williamson found XRD evidence for the onset of microcrystallinity, we found the appearance of the distinctive "shoulder" in our sub-band-gap photocapacitance spectra. Third, we investigated two sets of samples where the deposition rate had been varied to include samples grown at moderate to high rates. In one set of samples, produced at ETL, samples deposited under H ₂ dilution at 10 Å/s were found to exhibit extremely low deep defect densities and narrow Urbach tails, indicating films of exceptional quality. The photocapacitance spectra for these films were found to contain evidence for a small degree of microcrystallinity. In another set of samples, produced at UniSolar, we found evidence for increasing defect densities plus somewhat larger Urbach energies for the films deposited at higher rates. This is consistent with the fact that the photovoltaic device performance is significantly poorer for the higher deposition rate material. Finally, we discussed the general issue of deep defect densities in the a-Si,Ge:H alloys. We again demonstrated how well the deep defect densities in such samples from several sources could be fit using the spontaneous bond-breaking model of Martin Stutzmann. This implies that such state-of-the-art alloy films have been optimized in a quantifiable sense. We also found that the increase in deep defect density with small amounts of P and B dopants could also be reproduced reasonably well by modifying the spontaneous bond-breaking model to include the extra energy terms associated with charged defects.				
14. SUBJECT TERMS photovoltaics ; amorphous silicon ; mid-gap cells ; low-gap cells ; light-induced degradation ; defect behavior ; defect densities ; microcrystallinity			15. NUMBER OF PAGES	
			16. PRICE CODE	
17. SECURITY CLASSIFICATION OF REPORT Unclassified	18. SECURITY CLASSIFICATION OF THIS PAGE Unclassified	19. SECURITY CLASSIFICATION OF ABSTRACT Unclassified	20. LIMITATION OF ABSTRACT UL	